ELSEVIER

Comput. Methods Appl. Mech. Engrg. 190 (2001) 5867–5892

Computer methods in applied mechanics and engineering

www.elsevier.com/locate/cma

A finite element method for magnetohydrodynamics

Nizar Ben Salah [a], Azzeddine Soulaimani [a,*], Wagdi G. Habashi [b]

[a] *École de Technologie Supérieure, Département de Génie Mécanique, 1100 rue Notre-Dame Ouest, Montréal, Qué., Canada H3C 1K3*
[b] *Mechanical Engineering, Concordia University, Montréal, Qué., Canada H3C 1K3*

Received 22 December 1999; received in revised form 21 October 2000

Abstract

This paper presents a finite element method for the solution of 3D incompressible magnetohydrodynamic (MHD) flows. Two important issues are thoroughly addressed. First, appropriate formulations for the magnetic governing equations and the corresponding weak variational forms are discussed. The selected $(\mathbf{B}, q)$ formulation is conservative in the sense that the local divergence-free condition of the magnetic field is accounted for in the variational sense. A Galerkin-least-squares variational formulation is used allowing equal-order approximations for all unknowns. In the second issue, a solution algorithm is developed for the solution of the coupled problem which is valid for both high and low magnetic Reynolds numbers. Several numerical benchmark tests are carried out to assess the stability and accuracy of the finite element method and to test the behavior of the solution algorithm.

Keywords: Incompressible magnetohydrodynamics; Finite element methods; Hartmann flows; Segregated algorithm; ILUT; GMRES

0. Introduction

Despite the great development of computer resources and numerical methods in the two last decades, magnetohydrodynamic (MHD) research is still mainly analytical or experimental in nature although the absolute number of numerical articles on MHD has been constantly increasing. Research on MHD flows can be divided into two categories, inviscid compressible flows mainly concerned with plasmas and viscous incompressible flows for liquid metals.

For a review of the mathematical modeling and numerical methods of compressible inviscid MHD problems, see [1,2]. Numerical modeling of incompressible MHD flows has been done essentially in the framework of the development of a fusion reactor liquid–metal coolant and the revival of liquid–metal MHD electricity generation. These MHD problems have been extensively studied by the method of asymptotic expansions (see [3] for a review of the results of these studies). The obvious restrictions inherent in asymptotic methods have been partially overcome by the development of semi-numerical methods [4,5]. However, these methods are still unable to solve the boundary layers. These flow details could be obtained by means of a fully numerical approach. Yet, only a relatively small number of articles have used this approach mainly in one or two dimensions. For instance, Ramos and Winowich [6] proposed three numerical methods, a finite element formulation, a stream function-vorticity finite difference method and a control volume type scheme. Regarding electromagnetic quantities, they solved for the electric potential, while the imposed magnetic field is supposed to remain unperturbed. Scandiuzzi and Schrefler [7] presented a finite element method for solving 2D MHD flows. The method solves for the only non-zero component of

* Corresponding author. Tel.: +1-514-396-8977; fax: +1-514-396-8530.
E-mail address: asoulaimani@mec.etsmtl.ca (A. Soulaimani).

0045-7825/01/$ - see front matter
PII: S0045-7825(01)00196-7

the velocity and the magnetic field. For the boundary conditions on the magnetic field, an equation is developed relating the magnetic field component to the relative conductivity of the walls.

3D simulations of MHD incompressible flows are even more rare. From the 561 numerical MHD articles published during the nineties, only 56 have the keyword "3D or three dimension*". What follows here is an attempt to review the papers proposing models for solving 3D MHD flows.

Sterl [21] presented a finite difference method for MHD flows in rectangular ducts. The method decouples the magnetic field problem from the fluid by considering the limit that no perturbation is induced for the magnetic field. It solves for the velocity field and the electric scalar potential with **B**, the magnetic field, considered constant in the equations and presents results for 3D effects of the developing entry in rectangular ducts. Based on the work in [3], Sterl generalized the boundary conditions that have to be assigned for the electric potential ϕ in order to account for a varying relative conductivity ratio. Seungsoo and Dulikravich [22] proposed a finite difference method in the general non-orthogonal curvilinear boundary-conforming coordinate system. The solution algorithm is based on an explicit Runge–Kutta time-stepping scheme. This model solves for the velocity, the magnetic and the temperature fields and results were presented for the 3D Hartmann flow and Benard cell problem. The numerical results showed the magnetic weakening of the thermally induced vortices and the eventual damping of buoyancy movement when the Hartmann number is high ($Ha = 10,\ Gr = 3000$).

Dulikravich et al. [23] solved for the 3D laminar viscous flow undergoing solidification or melting under the influence of arbitrarily oriented externally applied magnetic field. The algorithm used is the same as in [22] with the difference that the magnetic field is decoupled from the velocity and the temperature fields for small magnetic Reynolds numbers ($Re_m \ll 1$) and the energy model accounts for a temperature dependence of the physical properties. In [24] another finite difference method for 3D MHD equations is presented. Numerical results concern the Hartmann–Poiseuille flow and the shielding skin effect.

Regarding the methodologies used for solving MHD equations, the finite element method has not been used as often as the finite difference or the finite volume methods. Peterson [25] studied theoretically a finite element formulation for steady incompressible flows of electrically conducting fluids by considering the special case of undisturbed external magnetic field. This study proved the stability, existence and uniqueness of the solution. Specifically, the electric scalar ϕ has to be chosen in the same functional subspace as the velocity field. For another kind of finite element approximations, Gardner and Gardner [26] presented a 2D bi-cubic B-spline finite element method for the MHD channel flow.

Solving the induction and the continuity equations for the magnetic field **B** would normally result in an over-determined system of equations. This problem can be overcome by dropping the continuity equation. The resulting vectorial equation is a diffusion–convection Helmholtz-like equation. While this is done in all the above references, it does not enforce the respect of one of the fundamental Maxwell equations. On the other hand, instead of choosing the magnetic field **B** as the main electromagnetic quantity, many authors choose to solve for the vector potential **A**, mostly in the context of pure electromagnetism. For a general overview of the vector potential methods and some of their electromagnetic applications, see [8].

In the context of MHD, vector potential methods have been popular and intensively used especially for metallurgical applications [27]. Fautrelle [9] used a vector potential formulation to solve the magnetic part of electromagnetic stirring problem. This method treated it as a pure electromagnetic problem by dropping the motion effects in the Maxwell equations. Mestel [10] examined analytically and numerically the process of levitation melting of metals. Lympany et al. [11] presented numerical results for the MHD effects in aluminum reduction cells. Assuming a steady 2D phenomenon, they solved for the scalar potential ϕ and deduced the magnetic field using the Biot–Savart law.

Besson et al. [12] developed a 2D steady-state finite element method for solving both the MHD and the free surface problems associated with electromagnetic casting (EMC). They represented the outside potential by an integral equation, so their method could be described as FEM/BEM. Conraths [13] described the magnetic field through an electric vector potential and a magnetic scalar potential for modeling an inductive heating device for thin moving metal strips.

Masse et al. [14] presented an impressive description of the main conclusions of ten years of numerical modeling in MHD using the vector potential formulations. Also, a methodology for solving coupled flows was proposed which combines different numerical approaches, a finite volume method for the fluid problem, a finite element method for the magnetic problem in the conducting domain and an integral

method for the non-conducting domain. While this literature survey is by no means exhaustive, it illustrates the general use of vector potential formulations and indicates their wide popularity.

The main idea behind vector potential methods is that since the magnetic field is solenoidal then it derives from a vector potential. Introducing this vector potential would then implicitly respect the free-divergence constraint on the magnetic field. To the best of our knowledge, only Oki and Tanahashi [29] have developed numerical schemes which explicitly satisfy the solenoidal condition of the magnetic field. They introduced a variable called hydro-magnetic cross-helicity $G = \mathbf{u} \cdot \mathbf{B}$ and retained the free-divergence equation within their system of equations. They presented results for the natural convection of a thermo-electrically conducting fluid under a magnetic field. Ben Salah et al. [19,20] have also explicitly respected the free-divergence condition by including it directly in the system of equations while overcoming the over-determination of the system.

As continuation of these previous works [19,20], this paper aims to develop a robust and cost-effective MHD algorithm that combines a Navier–Stokes flow solver and a magnetic solver for the solution of 3D MHD equations. Robustness is achieved by the solution of the two systems of equations in a fully coupled fashion.

The remainder of the paper is organized in five sections. In Section 1, the governing equations of MHD flows are reviewed. The Helmholtz formulation and the vector potential formulation of the magnetic induction are presented. Then, the conservative formulation is developed, which takes into account the explicit respect of the free-divergence constraint on the magnetic field by the numerical scheme. Section 2 deals with the variational formulations of the different systems of equations that are used throughout this paper. The Galerkin weak form of the $(\mathbf{B}, q)$ formulation is obtained, giving rise to a mixed finite element formulation. A stabilization technique is introduced to circumvent the usual Brezzi–Babuska stability condition and to allow equal interpolation for all the variables. A penalty factor is then introduced in order to force the magnetic divergence towards zero. For the vector potential formulation, the Galerkin weak form allows for the use of equal interpolation for all variables. Thus, no stabilization technique is required for such formulations. The Navier–Stokes equations are stabilized through a Galerkin-least-squares term. In Section 3, the solution strategy for the decoupled formulations $(\mathbf{B}, q)$ and $(\mathbf{A}, \phi)$ and the coupled formulation $(\mathbf{B}, q, \mathbf{u}, p)$ is presented. The strategy for the coupled problem is based on a non-linear GMRES algorithm associated with an ILUT preconditioning. The generic form of the segregated algorithm allows for the possibility to update the magnetic matrix whenever the physical parameters require such updating. In Section 4 several benchmark tests which concern the accuracy and stability of the different finite element methods are carried out. Further results are presented for the coupled formulation $(\mathbf{B}, q, \mathbf{u}, p)$ in order to assess the proposed solution algorithm robustness. In Section 6, main conclusions of this work and suggestions for future work are presented.

1. The governing equations

Under the classical MHD assumptions [18] and assuming the electric conductivity to be constant, the MHD set of equations can be recast as:

$$\frac{\partial \mathbf{B}}{\partial t} - \nabla \times (\mathbf{u} \times \mathbf{B}) + \eta \nabla \times (\nabla \times \mathbf{B}) = 0, \tag{1}$$

$$\nabla \cdot \mathbf{B} = 0, \tag{2}$$

where $\eta = 1/\mu\sigma$ is the magnetic diffusivity coefficient (μ and σ are, respectively, the magnetic permeability and the electric conductivity). In Eqs. (1) and (2), $\mathbf{B}$ and $\mathbf{u}$ are the magnetic and the velocity fields. Eq. (1) is the well-known form of the magnetic induction equation. It consists of a diffusive second-order curl–curl term, a convective first-order curl term and a hyperbolic in time first-order term. It brings the advantage of directly relating the main hydrodynamic quantity, the velocity field, to the main electromagnetic one, the magnetic field, without any interference. Eq. (2) expresses the continuity of the magnetic field and is one of the original Maxwell equations. Once Eqs. (1) and (2) are solved for the magnetic field, the electric field $\mathbf{E}$ can be deduced from the following equation:

$$\mathbf{E} = \eta(\nabla \times \mathbf{B}) - \mathbf{u} \times \mathbf{B}. \tag{3}$$

Here, it should be pointed out that the magnetic free-divergence constraint (2) is implicit in Eq. (1). Indeed, if the divergence of Eq. (1) is taken term by term the following condition on the divergence of $\mathbf{B}$ is obtained:

$$\frac{\partial(\nabla \cdot \mathbf{B})}{\partial t} = 0. \tag{4}$$

Eq. (4) stipulates that the divergence of $\mathbf{B}$ remains constant over time and thus zero if it is initially null. However, it is well known that the construction of such an initial divergence-free field is generally not an easy task. Moreover, although the local conservation of the magnetic field is included in (2), this property might not hold exactly for a discrete version developed for a numerical solution of the partial differential equations. Thus the resulting system of equations must consist of both Eqs. (1) and (2).

1.1. The "Helmholtz" formulation

As stated in Section 0, this formulation is widely used in the literature. The starting point of this formulation is Eqs. (1) and (2), then using the vector identity stating that

$$\nabla \times (\nabla \times \mathbf{B}) = -\nabla^2 \mathbf{B} + \nabla(\nabla \cdot \mathbf{B}) \tag{5}$$

and using Eq. (2), the following Helmholtz equation is obtained:

$$\frac{\partial \mathbf{B}}{\partial t} - \nabla \times (\mathbf{u} \times \mathbf{B}) - \eta \nabla^2 \mathbf{B} = 0, \tag{6}$$

hence reducing the MHD system of Eqs. (1) and (2) to Eq. (6) with the appropriate set of boundary conditions. It should be noted that circumventing the constraint (2) by solving Eq. (6) results in a much simpler system to solve. However, Eq. (6) no longer states that the divergence of $\mathbf{B}$ remains constant over time. It only states that

$$\frac{\partial(\nabla \cdot \mathbf{B})}{\partial t} = \nabla \cdot (\eta \nabla^2 \mathbf{B}). \tag{7}$$

This divergence can be expected to play a non-negligible role in the discrete form of the weak problem associated with the continuous strong problem (6).

Remark 1. We would like to point out here an analogy with the Stokes problem for an incompressible fluid with constant viscosity. The Stokes problem is written as:

$$-\nabla \cdot (2\eta\gamma(\mathbf{u})) + \nabla \mathbf{p} = \mathbf{f}, \tag{8}$$

$$\nabla \cdot \mathbf{u} = 0 \tag{9}$$

with η the dynamic viscosity coefficient and $\gamma(\mathbf{u})$ the symmetric part of the velocity gradient tensor. If one derives from (8) and (9), the equations for the special case of constant viscosity η, then by making use of Eq. (9), this results in

$$-\eta \nabla^2 \mathbf{u} + \nabla \mathbf{p} = \mathbf{f}. \tag{10}$$

Although Eq. (9) has been used in order to derive (10), it is well known that one has to keep the divergence-free constraint (9) within the system of equations while developing any numerical solution of the Stokes problem. The pressure p plays the role of a Lagrange multiplier in order to enforce the velocity divergence-free condition. This analogy is also valid for the Navier–Stokes equations. The magnetic continuity Eq. (2) is the electromagnetic equivalent of the hydrodynamic continuity Eq. (9) and deserves some attention.

1.2. The vector potential formulation

Alternatively to the above introduction of the magnetic induction equation which relates the magnetic and the velocity fields **B** and **u**, one can introduce a vector potential formulation. From Eq. (2), it is seen that the magnetic field results from a vector potential **A**

$$\nabla \times \mathbf{A} = \mathbf{B}. \tag{11}$$

Then Eq. (2) is automatically satisfied. Noting that the electric field is defined as

$$\mathbf{E} = -\nabla\phi - \frac{\partial \mathbf{A}}{\partial t}, \tag{12}$$

where ϕ is the scalar electric potential, one can write

$$\frac{\partial \mathbf{A}}{\partial t} - \mathbf{u} \times (\nabla \times \mathbf{A}) + \frac{1}{\mu\sigma}\nabla \times (\nabla \times \mathbf{A}) + \nabla\phi = 0. \tag{13}$$

This equation, known as the vector potential equation, shows that the time evolution of the vector potential is determined by the diffusion and the convection of the vector magnetic potential and by the scalar electric potential gradient. The fact that Eq. (13) defines only the curl of **A** implies that the vector potential is defined up to the gradient of an arbitrary scalar function (see [27]). It is classical in the electromagnetic context to use the Coulomb gauge defined as

$$\nabla \cdot \mathbf{A} = 0. \tag{14}$$

This gauge could be either imposed explicitly by adding Eq. (14) to Eq. (13) or as suggested by Biro and Preiss [8], by adding a penalty term to the vector potential equation (13)

$$\frac{\partial \mathbf{A}}{\partial t} - \mathbf{u} \times (\nabla \times \mathbf{A}) + \frac{1}{\mu\sigma}\nabla \times (\nabla \times \mathbf{A}) - \nabla\left(\frac{1}{\mu\sigma}\nabla \cdot \mathbf{A}\right) + \nabla\phi = 0. \tag{15}$$

In case of constant magnetic permeability, as under the MHD assumptions, and in case of constant conductivity, this results in the Laplacian operator replacing the curl–curl operator

$$\frac{\partial \mathbf{A}}{\partial t} - \mathbf{u} \times (\nabla \times \mathbf{A}) - \frac{1}{\mu\sigma}\nabla^2\mathbf{A} + \nabla\phi = 0. \tag{16}$$

The conservation of the electric current is implicit in the vector potential equation (13). Actually, taking the divergence of Eq. (13) term by term results in

$$\nabla \cdot \left(-\frac{\partial \mathbf{A}}{\partial t} - \nabla\phi + \mathbf{u} \times (\nabla \times \mathbf{A})\right) = 0. \tag{17}$$

However, this same conservation condition no longer follows from the modified vector potential equation (16). The electric current conservation (17) then has to be prescribed. Thus using the $(\mathbf{A}, \phi)$ formulation would result in the system of Eqs. (16) and (17).

1.2.1. Reduced vector potential formulation

As stated by Emson and Simkin [15], it is possible to define a new vector potential $\hat{\mathbf{A}}$ by the following equation:

$$\hat{\mathbf{A}} = \mathbf{A} + \int_t \nabla\phi \, \mathrm{d}t. \tag{18}$$

Then starting from the vector potential equation (13), one can obtain

$$\frac{\partial \hat{\mathbf{A}}}{\partial t} - \mathbf{u} \times (\nabla \times \hat{\mathbf{A}}) + \frac{1}{\mu\sigma}\nabla \times (\nabla \times \hat{\mathbf{A}}) = 0. \tag{19}$$

Emson noted that Eq. (19) has a unique solution with an implied coulomb gauge (14) which was therefore not imposed. As an alternative to Emson's method, one could follow the same procedure regarding the vector potential formulation by adding a penalty term to Eq. (19) in order to impose the divergence-free condition (14). This would yield, in the case of constant diffusivity, the following reduced vector potential equation:

$$\frac{\partial \hat{\mathbf{A}}}{\partial t} - \mathbf{u} \times (\nabla \times \hat{\mathbf{A}}) - \frac{1}{\mu\sigma}\nabla^2 \hat{\mathbf{A}} = 0. \tag{20}$$

1.3. The conservative formulation

The idea leading to the Helmholtz formulation is that the system (1) and (2) is over-specified. For example in the 3D case and if the velocity field is assumed known, the system leads to four linear equations with three unknowns. In [16], Jiang et al. showed that an equivalent situation exists in the pure electromagnetic context. By introducing two dummy scalar variables, they showed that the first-order div-curl Maxwell's system of equations is equivalent to a non-over-specified system of equations.

Following the same technique, we will show that the system (1) and (2) is equivalent to a non-over-specified system of equations. Let Ω be a bounded, simply connected, convex and open domain which is included in R^3, with a piecewise smooth boundary Γ, the union of Γ_1 and Γ_2, with $\mathbf{n}$ the unit normal outward vector. Let Eqs. (1) and (2) hold in the domain Ω and be associated with appropriate boundary conditions on Γ. Adding the gradient of a scalar variable q to Eq. (1) results in the following equation:

$$\frac{\partial \mathbf{B}}{\partial t} - \nabla \times (\mathbf{u} \times \mathbf{B}) + \eta \nabla \times (\nabla \times \mathbf{B}) + \nabla q = 0 \quad \text{in } \Omega. \tag{21}$$

Let the homogeneous Dirichlet condition

$$q = 0 \tag{22}$$

hold on the boundary Γ. Taking the divergence of Eq. (21) and using Eq. (2) results in

$$\Delta q = 0 \quad \text{in } \Omega. \tag{23}$$

As Eq. (23) is subjected to the boundary condition (22), this leads to the unique physical solution $q = 0$ over all the domain Ω. Thus the scalar q is really a dummy variable (which in theory should be null) and the system of Eqs. (2) and (21) is equivalent to the system (1) and (2). The new system of equations has in the 3D case, four equations with four unknowns and is no longer over-determined. By analogy to the Stokes and the Navier–Stokes equations, q is interpreted as a Lagrange multiplier used to enforce the divergence-free condition (2).

Remark 2. Eq. (21) could be rewritten in many equivalent forms. Specifically, the following equivalent equation is obtained:

$$\frac{\partial \mathbf{B}}{\partial t} - \nabla \times (\mathbf{u} \times \mathbf{B}) - \eta \nabla^2 \mathbf{B} + \eta \nabla(\nabla \cdot \mathbf{B}) + \nabla q = 0 \quad \text{in } \Omega. \tag{24}$$

In the remainder of the paper, when we refer to the $(\mathbf{B}, q)$ formulation, we would be referring to the system of equations (2) and (24).

Remark 3. It is easily predictable that the non-explicit respect of the constraint (2) could lead to inaccurate numerical solutions. In order to show this, suppose one discards the divergence-free equation and retains only Eq. (1). For simplicity, let the velocity field be equal to zero and assume the problem to be steady. From (1), one obtains

$$\nabla \times (\nabla \times \mathbf{B}) = 0 \quad \text{in } \Omega \tag{25}$$

with the most probable boundary conditions

$$\mathbf{n}\cdot\mathbf{B}=0 \quad \text{on } \Gamma_1, \tag{26}$$

$$\mathbf{n}\times\mathbf{B}=0 \quad \text{on } \Gamma_2. \tag{27}$$

The solution of Eq. (25), subject to the boundary conditions (26) and (27), is not unique. It admits a kernel composed of the gradient of scalar variables satisfying the conditions (26) and (27). Any numerical method for problem (25)–(27) will fail to provide a unique solution. The constraint (2) should thus be taken into account and it behaves like a gauge condition filtering the divergence-free solution. The respect of this condition reduces the kernel of spurious solutions to a unique null scalar function.

Indeed, according to the unity partition theorem [17], there exist scalar functions ϕ that are C^∞, satisfying $\partial\phi/\partial n=0$ on Γ_1, $\mathbf{n}\times\nabla\phi=0$ on Γ_2 and ϕ non-null in a part of Ω. Thus if $\mathbf{B_0}$ is a particular solution of (25)–(27) then any vector $\mathbf{B}=\mathbf{B_0}+\nabla\phi$ is also a solution. But if the vector solution has to satisfy the divergence-free condition, then $\Delta\phi=0$ in Ω. As $\partial\phi/\partial n=0$ on Γ_1 and $\mathbf{n}\times\nabla\phi=0$ on Γ_2, then ϕ is equal to a constant in Ω. Since ϕ is prescribed zero over part of the domain, then $\phi=0$ over all the domain Ω.

1.4. The MHD equations

The mass and momentum conservations equations are written for an incompressible fluid as

$$\nabla\cdot\mathbf{u}=0, \tag{28}$$

$$\frac{\partial\mathbf{u}}{\partial t}+(\mathbf{u}\cdot\nabla)\mathbf{u}-\nu\nabla^2\mathbf{u}+\frac{1}{\rho}\nabla p=\mathbf{f}, \tag{29}$$

where p, ρ, ν and $\mathbf{f}$ are, respectively, the pressure, density, kinematic viscosity and body force field. For MHD problems, the body force term is $\mathbf{f}=\frac{1}{\rho}(\mathbf{j}\times\mathbf{B})$, and represents the Lorentz forces due to the interaction between the current density and the magnetic field. Replacing the current density by its expression gives

$$\frac{\partial\mathbf{u}}{\partial t}+(\mathbf{u}\cdot\nabla)\mathbf{u}-\nu\nabla^2\mathbf{u}+\frac{1}{\rho}\nabla p-\frac{1}{\mu\rho}(\nabla\times\mathbf{B})\times\mathbf{B}=0. \tag{30}$$

Eqs. (2) and (24) along with Eqs. (28) and (30) represent the governing equations that should ideally be resolved in order to describe properly any MHD phenomenon. These equations are fully coupled, since a two-way coupling exists between the fluid and the electromagnetic fields. The non-dimensional form of equations assesses the relative influence of the terms through which the coupling is exerted and is written:

$$\frac{\partial\mathbf{u}^*}{\partial t}+(\mathbf{u}^*\cdot\nabla)\mathbf{u}^*-\frac{1}{Re}\nabla^2\mathbf{u}^*+\nabla p^*-\frac{Ha^2}{ReRe_{\mathrm{m}}}(\nabla\times\mathbf{B}^*)\times\mathbf{B}^*=0, \tag{31}$$

$$\nabla\cdot\mathbf{u}^*=0, \tag{32}$$

$$\frac{\partial\mathbf{B}^*}{\partial t^*}-\nabla\times(\mathbf{u}^*\times\mathbf{B}^*)+\frac{1}{Re_{\mathrm{m}}}\nabla\times(\nabla\times\mathbf{B}^*)+\nabla q^*=0, \tag{33}$$

$$\nabla\cdot\mathbf{B}^*=0, \tag{34}$$

where the magnetic Reynolds number Re_{m} and the Hartmann number Ha are

$$Re_{\mathrm{m}}=\mu\sigma u_0 L, \quad Ha=B_0 L\left(\frac{\sigma}{\rho\nu}\right)^{1/2} \tag{35}$$

and, respectively, measure the relative importance of the convection of the magnetic field to its diffusion, and the relative importance of the electromagnetic forces to the viscous ones.

2. Variational formulations and finite element discretization

The Galerkin weighted residual formulations are obtained by multiplying the equations by test functions, respectively, chosen in appropriate functional spaces. Generally, these formulations are of mixed type and hence require the respect of the usual stability conditions [31]. An alternative way of obtaining stable finite element formulations, is to circumvent the L.B.B. conditions by using for instance the Galerkin-least-squares method [32].

2.1. The stabilized finite element method for the conservative formulation

Suppose $\Omega_h = \cup\Omega_e$, a certain partition of the domain Ω into elements and h the "size" of an element Ω_e. Following Brezzi and Pitkaranta [30], the stabilized weak discretized form for the conservative formulation (2) and (24) can be introduced as:

$$\int_\Omega \mathbf{B}_\mathbf{h}^* \cdot \frac{\partial \mathbf{B}_\mathbf{h}}{\partial t}\,d\Omega + \int_\Omega \eta \nabla \mathbf{B}_\mathbf{h}^* \cdot \nabla \mathbf{B}_\mathbf{h}\,d\Omega - \int_\Omega \mathbf{B}_\mathbf{h}^* \cdot \nabla \times (\mathbf{u} \times \mathbf{B}_\mathbf{h})\,d\Omega + \int_\Omega \mathbf{B}_\mathbf{h}^* \cdot \nabla q_h\,d\Omega$$
$$- \int_\Omega \eta(\nabla \cdot \mathbf{B}_\mathbf{h})(\nabla \cdot \mathbf{B}_\mathbf{h}^*)\,d\Omega - \int_\Gamma \eta(\mathbf{n} \cdot \nabla \mathbf{B}_\mathbf{h}) \cdot \mathbf{B}_\mathbf{h}^*\,d\Gamma + \int_\Gamma \eta(\mathbf{n} \cdot \mathbf{B}_\mathbf{h}^*)(\nabla \cdot \mathbf{B}_\mathbf{h})\,d\Gamma = 0, \tag{36}$$

$$\int_\Omega q_h^*(\nabla \cdot \mathbf{B}_\mathbf{h})\,d\Omega + \sum_{\Omega_e \in \Gamma_h} \int_{\Omega_e} \tau_1 \nabla q_h \cdot \nabla q_h^*\,d\Omega = 0, \tag{37}$$

where $\mathbf{B}_\mathbf{h}^*$ and q_h^* are test functions belonging to appropriate functional spaces and τ_1 is a function of the mesh size h that can be set to

$$\tau_1 = \alpha \frac{h^2}{4\eta} \tag{38}$$

or to

$$\tau_1 = \alpha \left(\left(\frac{2||\mathbf{u}||}{h} \right)^2 + \left(\frac{4\eta}{h^2} \right)^2 \right)^{-1/2}. \tag{39}$$

This formulation (36) and (37) creates the necessary coupling between the induction and the continuity equations. This coupling can be seen as the counterpart to the use of staggered grids in finite difference schemes. Once the stability of the formulation is insured, the volume integral emanating from the $\nabla(\nabla \cdot \mathbf{B})$ term is penalized with a term τ_2, in order to enforce the magnetic divergence towards small values when the convection is dominant (i.e. small values of η). Then the formulation reads as

$$\int_\Omega \mathbf{B}_\mathbf{h}^* \cdot \left(\frac{\partial \mathbf{B}_\mathbf{h}}{\partial t} \right) d\Omega + \int_\Omega \eta \nabla \mathbf{B}_\mathbf{h}^* \cdot \nabla \mathbf{B}_\mathbf{h}\,d\Omega - \int_\Omega \mathbf{B}_\mathbf{h}^* \cdot \nabla \times (\mathbf{u} \times \mathbf{B}_\mathbf{h})\,d\Omega + \int_\Omega \mathbf{B}_\mathbf{h}^* \cdot \nabla q_h\,d\Omega$$
$$+ \int_\Omega (\tau_2 - \eta)(\nabla \cdot \mathbf{B}_\mathbf{h})(\nabla \cdot \mathbf{B}_\mathbf{h}^*)\,d\Omega - \int_\Gamma \eta(\mathbf{n} \cdot \nabla \mathbf{B}_\mathbf{h}) \cdot \mathbf{B}_\mathbf{h}^*\,d\Gamma + \int_\Gamma \eta(\mathbf{n} \cdot \mathbf{B}_\mathbf{h}^*)(\nabla \cdot \mathbf{B}_\mathbf{h})\,d\Gamma = 0, \tag{40}$$

$$\int_\Omega q_h^*(\nabla \cdot \mathbf{B}_\mathbf{h})\,d\Omega + \sum_{\Omega_e \in \Gamma_h} \tau_1 \int_{\Omega_e} \tau_1 \nabla q_h \cdot \nabla q_h^*\,d\Omega = 0, \tag{41}$$

where τ_2 is set to either

$$\tau_2 = 0, \tag{42}$$

which corresponds to the original physical model, or to

$$\tau_2 = ||\mathbf{u}||h/2. \tag{43}$$

In the latter case, the coefficient $r = \tau_2 - \eta$ ends up to be $r = \eta(1 - (Re_{m_h}/2))$, where $Re_m h = \sigma\mu||\mathbf{u}||h$ is the local magnetic Reynolds number. The stabilized method defined by (40) and (41) allows for the use of equal

interpolation for the two variables $(\mathbf{B}_\mathbf{h}^*, \mathbf{q}_\mathbf{h}^*)$, thus facilitating the implementation and permitting the use of elements less costly in terms of calculations.

2.2. Galerkin method for the vector potential formulation

The discretized Galerkin weighted residual formulation for the system of equations (16) and (17) is presented as:

$$\int_\Omega \mathbf{A}_\mathbf{h}^* \cdot \frac{\partial \mathbf{A}_\mathbf{h}}{\partial t}\,\mathrm{d}\Omega + \int_\Omega \eta \nabla \mathbf{A}_\mathbf{h}^* \cdot \nabla \mathbf{A}_\mathbf{h}\,\mathrm{d}\Omega + \int_\Omega \mathbf{A}_\mathbf{h}^* \cdot \nabla \phi_h\,\mathrm{d}\Omega - \int_\Omega \mathbf{A}_\mathbf{h}^* \cdot \mathbf{u}_\mathbf{h} \times (\nabla \times \mathbf{A}_\mathbf{h})\,\mathrm{d}\Omega - \int_\Gamma \eta(\mathbf{n} \cdot \nabla \mathbf{A}_\mathbf{h}) \cdot \mathbf{A}_\mathbf{h}^*\,\mathrm{d}\Gamma = 0, \tag{44}$$

$$\int_\Omega \left(\frac{\partial \mathbf{A}_\mathbf{h}}{\partial t} - \mathbf{u}_\mathbf{h} \times (\nabla \times \mathbf{A}_\mathbf{h}) + \nabla \phi_h \right) \cdot \nabla \phi_h^*\,\mathrm{d}\Omega + \int_\Gamma (\mathbf{j}_\mathbf{h} \cdot \mathbf{n}) \cdot \phi_h^*\,\mathrm{d}\Gamma = 0. \tag{45}$$

Since Eqs. (16) and (17) include second-order terms both in $\mathbf{A}$ and ϕ, the formulation (44) and (45) does not need additional stabilizing terms to allow equal interpolation for the variables $(\mathbf{A}, \phi)$.

2.3. Galerkin method for the reduced vector potential equation

The discrete weak Galerkin form for the reduced vector potential equation (20) is presented as

$$\int_\Omega \hat{\mathbf{A}}_h^* \cdot \left(\frac{\partial \hat{\mathbf{A}}_h}{\partial t} - \mathbf{u}_\mathbf{h} \times (\nabla \times \hat{\mathbf{A}}_h) \right) \mathrm{d}\Omega + \int_\Omega \eta \nabla \hat{\mathbf{A}}_h^* \cdot \nabla \hat{\mathbf{A}}_h\,\mathrm{d}\Omega - \int_\Gamma \eta(\mathbf{n} \cdot \nabla \hat{\mathbf{A}}_h) \cdot \hat{\mathbf{A}}_h^*\,\mathrm{d}\Gamma = 0 \tag{46}$$

for all $\hat{\mathbf{A}}_h^*$ belonging to some finite-dimensional sub-spaces.

2.4. Galerkin-least-squares formulation

In the context of fluid mechanics, Galerkin-least-squares formulations [33] have been used successfully by many authors, in order to ensure both the stabilization for equal-order interpolation and for high Reynolds numbers. In this case, such formulation is presented in the following compact form as

$$\begin{aligned}
&\int_\Omega \mathbf{v}_\mathbf{h} \cdot \left(\frac{\partial \mathbf{u}_\mathbf{h}}{\partial t} + (\mathbf{u}_\mathbf{h} \cdot \nabla)\mathbf{u}_\mathbf{h} \right) \mathrm{d}\Omega + \nu \int_\Omega \nabla \mathbf{u}_\mathbf{h} \cdot \nabla \mathbf{v}_\mathbf{h}\,\mathrm{d}\Omega - \frac{1}{\rho} \int_\Omega p_h \nabla \cdot \mathbf{v}_\mathbf{h}\,\mathrm{d}\Omega \\
&+ \sum_{\Omega_\mathrm{e} \in \Omega_h} \int_{\Omega_\mathrm{e}} \tau_1 \left(\frac{\partial \mathbf{u}_\mathbf{h}}{\partial t} + (\mathbf{u}_\mathbf{h} \cdot \nabla)\mathbf{u}_\mathbf{h} - \nu \nabla^2 \mathbf{u}_\mathbf{h} + \frac{1}{\rho} \nabla p_h \right) \cdot \left((\mathbf{u}_\mathbf{h} \cdot \nabla)\mathbf{v}_\mathbf{h} + \nu \nabla^2 \mathbf{v}_\mathbf{h} + \frac{1}{\rho} \nabla p_h^* \right) \mathrm{d}\Omega_\mathrm{e} \\
&- \int_\Omega \frac{1}{\mu} ((\nabla \times \mathbf{B}_\mathbf{h}) \times \mathbf{B}_\mathbf{h}) \cdot \mathbf{v}_\mathbf{h}\,\mathrm{d}\Omega + \frac{1}{\rho} \int_\Gamma p_h \mathbf{v}_\mathbf{h} \cdot \mathbf{n}\,\mathrm{d}\Gamma - \nu \int_\Gamma (\nabla \mathbf{u}_\mathbf{h} \cdot \mathbf{n}) \cdot \mathbf{v}_\mathbf{h}\,\mathrm{d}\Gamma + \int_\Omega p_h^* (\nabla \cdot \mathbf{u}_\mathbf{h})\,\mathrm{d}\Omega = 0
\end{aligned} \tag{47}$$

From the above stabilized formulation, one can obtain the corresponding momentum equations by choosing $p_h^* = 0$, or obtain the corresponding continuity equation for $\mathbf{v}_\mathbf{h} = 0$.

Remark 4. If the test and the shape functions are interpolated on a linear basis, then the second-order terms appearing in the stabilization terms of (47) cancel and the formulation simplifies to

$$\begin{aligned}
&\int_\Omega \mathbf{v}_\mathbf{h} \cdot \left(\frac{\partial \mathbf{u}_\mathbf{h}}{\partial t} + (\mathbf{u}_\mathbf{h} \cdot \nabla)\mathbf{u}_\mathbf{h} \right) \mathrm{d}\Omega + \nu \int_\Omega \nabla \mathbf{u}_\mathbf{h} \cdot \nabla \mathbf{v}_\mathbf{h}\,\mathrm{d}\Omega - \frac{1}{\rho} \int_\Omega p_h \nabla \cdot \mathbf{v}_\mathbf{h}\,\mathrm{d}\Omega \\
&+ \sum_{\Omega_\mathrm{e} \in \Omega_h} \int_{\Omega_\mathrm{e}} \tau_1 \left(\frac{\partial \mathbf{u}_\mathbf{h}}{\partial t} + (\mathbf{u}_\mathbf{h} \cdot \nabla)\mathbf{u}_\mathbf{h} + \frac{1}{\rho} \nabla p_h \right) \cdot \left((\mathbf{u}_\mathbf{h} \cdot \nabla)\mathbf{v}_\mathbf{h} + \frac{1}{\rho} \nabla p_h^* \right) \mathrm{d}\Omega_\mathrm{e} + \int_\Omega p_h^* (\nabla \cdot \mathbf{u}_\mathbf{h})\,\mathrm{d}\Omega \\
&- \int_\Omega \frac{1}{\mu} ((\nabla \times \mathbf{B}_\mathbf{h}) \times \mathbf{B}_\mathbf{h}) \cdot \mathbf{v}_\mathbf{h}\,\mathrm{d}\Omega + \frac{1}{\rho} \int_\Gamma p_h \mathbf{v}_\mathbf{h} \cdot \mathbf{n}\,\mathrm{d}\Gamma - \nu \int_\Gamma (\nabla \mathbf{u}_\mathbf{h} \cdot \mathbf{n}) \cdot \mathbf{v}_\mathbf{h}\,\mathrm{d}\Gamma = 0.
\end{aligned} \tag{48}$$

In the rest of the paper the test and the shape functions are interpolated on linear tetrahedral elements. The time derivative vectors are evaluated by a finite difference-like expression. Using the second-order Gear scheme, any unknown vector $\dot{U}$ is written as

$$\dot{U} = \frac{3U_n - 4U_{n-1} + U_{n-2}}{2\Delta t}. \tag{49}$$

Such a scheme requires solution vectors at two time steps $n-2$ and $n-1$, in order to be implemented. During the first time step, the first-order implicit Euler scheme is used

$$\dot{U} = \frac{U_n - U_{n-1}}{\Delta t}. \tag{50}$$

3. Solution strategies

After time and space discretizations, the variational problems (40) and (41), (44) and (45) (or (46)) and (47) are equivalent to solving linear or non-linear sets of equations depending whether the magnetic problem, the fluid problem or both of them are solved. Here we chose to develop a two-steps approach: in the first one, the magnetic problem ((40) and (41), (44) and (45) or (46)) is decoupled from the fluid problem with the velocity given as data to the magnetic problem. In the second step, the coupled problem (40) and (41) and (47) is solved. Thus two solvers (the fluid solver and the magnetic one) and a coupling algorithm are involved in the solution strategies.

3.1. The fluid solver

The non-linear set of equations arising from the variational statement (47) can be put in the following generic form:

$$[K(U)]\{U\} = \{F(U,B)\}, \tag{51}$$

where $[K(U)]$, $\{F(U,B)\}$ and $\{U\}$ are, respectively, the global matrix, the global right-hand side vector and the global nodal variables, corresponding to the fluid problem. In order to solve such a non-linear system, one has to linearize it, for instance using Newton method which consists of solving the alternative linear system

$$\left[J(U^{n,i-1})\right]\{\Delta U^{n,i}\} = -\left\{R(U^{n,i-1}, B^n)\right\}, \tag{52}$$

where $\{U^{n,i}\}$ and $\{B^n\}$ are, respectively, the global solution vectors for the fluid problem at time step n and iteration i and for the magnetic problem at time step n, $\{R\}$ is the residual vector and $[J]$ is the Jacobian matrix.

Algorithm 1 (*Newton–Raphson*).

1. Given an initial solution $\{U^0\}$,
2. For $n = 1, 2, \ldots$ do:
3. $\{U\}^{n,0} = \{U\}^{n-1}$,
4. For $i = 1, 2, \ldots$ do:
5. Compute $[J(U^{n,i-1})]$ and $\{R(U^{n,i-1}, B^n)\}$,
6. Solve the linear system (52),
7. Update $\{U^{n,i}\} = \{U^{n,i-1}\} + \{\Delta U^{n,i}\}$,
8. If convergence criterion is satisfied goto 10,
9. End of Newton iterations,
10. End of time iterations.

In the above algorithm, most of computations and storage requirements are implied by the way the linear system (52) is solved. Since the Jacobian matrix is sparse and non-symmetric and for large-scale

systems, among Krylov space iterative methods, the GMRES algorithm has proved to be an interesting option [35].

3.2. ILUT preconditioning

One can distinguish two classes of incomplete LU factorization preconditionings [34]:

1. The zero–non-zero structure of $[L]+[U]$ is the same as the original matrix $[A]$, i.e., m_{ij} is a non-zero coefficient of $[M]=[L]+[U]$, the preconditioning matrix, if and only if a_{ij} itself is non-zero.
2. A certain amount of fill-in is allowed to take place in the structure of $[L]+[U]$. In the limit of large fill-in amount, the factorization of $[A]$ becomes complete.

ILU(0) is a representative of the first class [36]. More recently, Saad [37,38] developed the very promising ILUT method. The preconditioning matrix is obtained by constructing $[L]$ and $[U]$ subject to the restriction that for each row of both triangular matrices, only a controlled amount of non-zero coefficients are allowed in $[L]$ and $[U]$ during the Gauss elimination. Furthermore, coefficients of the matrix deemed to bring an insignificant contribution to the incomplete decomposition are dropped. Thus, two values characterize the ILUT method: an integer one, *lfil*, for the number of non-zero coefficients per row and a real one, *tol*, which is a criterion to measure the influence of a coefficient on the incomplete LU decomposition. Both *lfil* and *tol* are to be set by the user.

Algorithm 2 (*ILUT*).

1. do $i=1,n$
2. do $k=1,i-1$
3. $J_{i,k}=J_{i,k}/J_{k,k}$
4. If $J_{i,k}$ is not too small then do $j=k+1,n$
5. $J_{i,j}=J_{i,j}-J_{i,k}*J_{k,j}$
6. enddo
7. enddo
8. Drop small elements in row $J_{i,*}$
9. enddo

As a result, the ILUT preconditioned Newton-GMRES algorithm reads as:

Algorithm 3 (*Newton-GMRES/ILUT*).

1. Given an initial solution U^0 do,
2. For $n=1,2,\ldots$ do:
3. $\{U\}^{n,0}=\{U\}^{n-1}$,
4. Compute J and its ILUT factorization,
5. For $i=1,\ldots,max-iteration$, do:
6. Compute $M^{-1}\cdot J$ and $M^{-1}\cdot\{R\}$,
7. run GMRES to solve system (52),
8. Update $\{U^{n,i}\}=\{U^{n,i-1}\}+\{\Delta U^{n,i}\}$,
9. if convergence criteria are satisfied goto 11,
10. enddo
11. enddo

An important aspect of the GMRES algorithm is that it only requires the dot product of the Jacobian matrix by a vector. This operation can be approximated by the following difference quotient

$$J(\{U\}^{n,i-1})\cdot\{v\}=\frac{\{R\}(\{U\}^{n,i-1}+\sigma\{v\})-\{R\}(\{U\}^{n,i-1})}{\sigma}, \tag{53}$$

where σ is a small scalar to be specified.

3.3. The magnetic solver

Both the conservative formulation $(\mathbf{B}, q)$ and the vector potential formulation $(\mathbf{A}, \phi)$ (or the reduced vector potential $\hat{\mathbf{A}}$ formulation) give rise to a system of N equations which reads in the generic following form as

$$\big[K'(U)\big]\{B\} = \big\{F'(B,U)\big\}, \tag{54}$$

where $[K'(U)]$, $\{F'(B,U)\}$ and $\{B\}$ are, respectively, the global matrix, the global right-hand side vector and the global nodal variables.

For relatively large problems, it is preferable to solve problem (54) by an iterative solver. However, for our academic purposes and since the system is linear, a direct solver, based on the well-known Gauss elimination, is still a reasonable strategy for the resolution of system (54).

4. The coupling strategy

The fully coupled problem is described in its weak form by the variational statements (40) and (41), and (47). We chose this formulation rather than any other coupled formulation (implying the vector potential) because it has the advantage of directly relating the main hydrodynamic quantity (the velocity field) with the main electromagnetic one (the magnetic field). As an alternative to the simultaneous solution approach, which would require huge computational requirements in terms of memory and computational time, one can use a segregated scheme.

Segregated methods consist of a sequence of solutions of the two problems. The process is terminated when a certain convergence criterion is achieved during the iterative process. For time-dependent problems, coupling iterations are actually time steps and convergence is achieved when steady-state solutions are obtained. The generic form of the segregated algorithm could then be presented as:

Algorithm 4 (*generic form of the segregated algorithm*).

1- Choose initial solutions $\{U^0\}$ and $\{B^0\}$ and convergence criterion ϵ

2- Time Steps: For $i = 1, 2, \ldots, n$ steps

-2.1. Solve the Magnetic Problem:

$$\big[K'(U^m)\big]\{\Delta B^i\} = -\big\{R'(B^{i-1}, U^{i-1})\big\}.$$

-2.2. Update the Magnetic solution:

$$\{B^i\} = \big\{B^{i-1}\big\} + \{\Delta B^i\}.$$

-2.3. Solve the Fluid Problem:

$$[K(U^i)]\{\Delta U^i\} = -\big\{R(U^{i-1}, B^n)\big\}.$$

-2.4. Update the Fluid Solution:

$$\{U^i\} = \big\{U^{i-1}\big\} + \{\Delta U^i\}.$$

-2.5. If $\|\{R(U^i, B^n)\}\|_2 \leqslant \epsilon$ Stop

3- End of Time Steps

4- End

In the above algorithm, $\{U^m\}$ and $\{B^n\}$ are, respectively, the fluid and the magnetic solutions at certain previous mth and nth iterations with $m < i$ and $n \leqslant i$. Letting m take different values among $0, 1, \ldots, i$ and n take different values among $0, 1, 2, \ldots, i-1$, leads to a whole family of explicit schemes. For instance, setting $m = i-1$ and $n = i$ gives the simplest segregated algorithm. "Simplest" means the most obvious algorithm, in the algorithmic sense.

Steps (2.1) and (2.2) in the segregated algorithm, consist of solving and updating the magnetic solution. It was already seen that the direct solver chosen for the solution of the magnetic problem is still an acceptable strategy when the magnetic problem is decoupled from the fluid one. However, when the fluid and the magnetic problems are coupled, this strategy is no longer practical because it would involve the complete LU decomposition of the magnetic matrix at each time step of the segregated algorithm. One should then look for another strategy which would imply both reasonable computational requirements and robustness of algorithm.

One way to satisfy these two requirements is to make m take other values than $i-1$. This amounts to freezing the magnetic matrix $[K'(U^m)]$ for a certain number l of time steps. This, however, lags the magnetic matrix behind the residual magnetic vector thus requiring the implementation of an inner iteration for the magnetic problem. This inner iteration could be seen as a fixed-point method or as a Modified Newton method for the linear magnetic problem. In such case, the segregated algorithm becomes:

Algorithm 5 (*segregated algorithm with inner magnetic iterations*).

1- Choose initial solutions $\{U^0\}$ and $\{B^0\}$ and convergence criterion ϵ.
2- Compute the LU decomposition of the matrix $[K'(U^0)] = [L][U]$.
3- Time Steps: For i $= 1, 2, \ldots, n$ steps

-3.1. If $(i.mod.m) = 0$ and $m \neq 0$ compute $[L][U] = [K'(U^i)]$
-3.2. Set $\{B_0^{i-1}\} = \{B^{i-1}\}$
-3.3. Inner Magnetic Iterations: For $j = 1, \ldots, n$iter
-3.3.1. Solve the Magnetic Problem:

$$[L][U]\left\{\Delta B_j^{i-1}\right\} = -\left\{R'(B_{j-1}^{i-1}, U^{i-1})\right\}.$$

-3.3.2. Update the Inner magnetic Solution:

$$\left\{B_j^{i-1}\right\} = \left\{B_{j-1}^{i-1}\right\} + \left\{\Delta B_j^{i-1}\right\}.$$

-3.3.3. If $||\{R'(B_j^{i-1}, U^{i-1})\}||_2 \leqslant \epsilon$ Stop
-3.4. End of Magnetic Iterations
-3.5. Update Magnetic Field:

$$\{B^i\} = \left\{B_j^{i-1}\right\}$$

-3.6. Solve the Fluid Problem:

$$[K(U^i)]\{\Delta U^i\} = -\left\{R(U^{i-1}, B^i)\right\}.$$

-3.7. Update the Fluid Solution:

$$\{U^i\} = \left\{U^{i-1}\right\} + \{\Delta U^i\}.$$

-3.8. Convergence Test: If $||\{R(U^i, B^i)\}||_2 \leqslant \epsilon$
4- End of Time Steps
5- End

In the above algorithm, the updating of the magnetic matrix takes place only when needed. This property is highly desired in order to take into account both low and high magnetic Reynolds numbers Re_m. In fact, as discussed in Section (2.7), when diffusion is the dominant mechanism by which the magnetic field is transported, a certain decoupling exists between the magnetic field and the fluid one. Setting $m = 0$ is sufficient for the convergence of the segregated algorithm while resulting in a once and for all decomposition of the magnetic matrix.

However, when the magnetic Reynolds number Re_m is high, the magnetic matrix must be updated more frequently. In fact, in such cases, the magnetic field is frozen in the velocity field (in the physical sense), and any change in the fluid field is immediately captured by the magnetic field. Thus, freezing the magnetic matrix (with the initial velocity field) results in the divergence of the algorithm. Hence, m can no longer be set to zero. The choice of m as an updating criterion depends on the magnetic Reynolds number Re_m. The higher the magnetic Reynolds is, the more frequent the necessary updating of the matrix.

The algorithm described above can be seen as a compromise between and as a mixture of modified Newton method where the matrix is decomposed once and for all, and an exact Newton method where the matrix is updated at each iteration.

5. Numerical results

In [19], we presented numerical results concerning the $(\mathbf{B}, q)$ decoupled formulation. These results were conducted to assess stability and accuracy as well as to validate the numerical code developed for the decoupled finite element formulation (40) and (41). Though these tests are well described in [28] here we would like to reassess their main conclusions which can be summarized as:

- When the magnetic convection is the dominant mechanism, the optimal convergence rates and the more conservative and accurate formulations are obtained with $\tau_2 = ||\mathbf{u}||h/2$ and

$$\tau_1 = \alpha\left(\left(\frac{2||\mathbf{u}||}{h}\right)^2 + \left(\frac{4\eta}{h^2}\right)^2\right)^{-1/2}$$

  with $\alpha = 0.1$.
- When the magnetic diffusion is the dominant mechanism, using $\tau_2 = 0$ and $\tau_1 = \alpha\frac{h^2}{4\eta}$ with $\alpha = 0.1$ gives the best numerical results.
- The Hartmann–Poiseuille flow and the Rayleigh–Hartmann test cases display two unique MHD physical features, namely, the building of the Hartmann layer and the development of Alfven waves, and show quite good agreement with analytical solutions.

The Hartmann–Poiseuille and Hartmann–Rayleigh tests are one-directional and in the next section, we present a 3D numerical test for the decoupled $\mathbf{B}, q$ formulation.

5.1. Lid-driven cavity problem for the decoupled formulation $\mathbf{B}, q$

Let the domain of study be a cubic unity domain ($0 \leqslant x \leqslant 1$, $0 \leqslant y \leqslant 1$, $0 \leqslant z \leqslant 1$). Suppose the hydrodynamic solution of the classical lid-driven cavity problem at a certain Reynolds number Re is given as input data. Suppose then that a transverse uniform magnetic field $\mathbf{B_0}$ is imposed in the y direction (Fig. 1).

The 3D velocity field will convect the magnetic field through its lines and its capacity to do so depends on the magnetic Reynolds number, Re_m. When Re_m is low, the magnetic field is transported in a quasi-pure diffusive manner. The convection of the magnetic field by the velocity could hence be neglected. As the magnetic Reynolds number increases, the convection of the magnetic field becomes more important. When Re_m is high enough, the convection of the magnetic field becomes the dominant regime of the transport mechanism and the magnetic field is said to be "frozen" in the velocity field.

Computations have been carried out in the above-described geometry for different magnetic Reynolds numbers ($Re_m = 0.1$, 1, 10, 100, 400, 1000). An unstructured coarse mesh consisting of 41 873 elements and 8147 nodes is used. In each case, we seek the steady-state solution. The velocity field given as input data

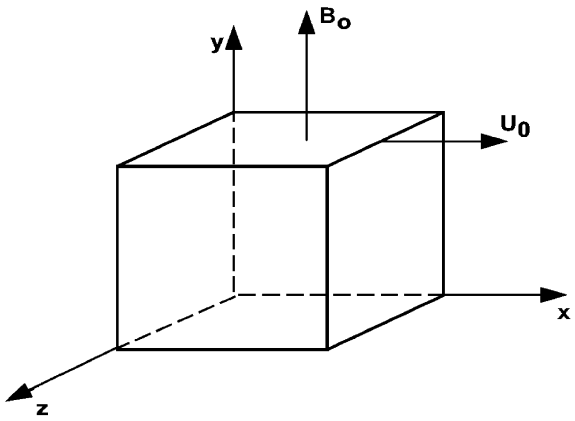

Fig. 1. Geometry for the cavity-driven problem.

represents the hydrodynamic solution for $Re = 400$. Dirichlet boundary conditions are imposed, thus representing the non-perturbation of the external magnetic field by the internal induced one. The computed solutions show the gradual evolution of the magnetic field transport from a quasi-diffusive regime to a quasi-convective one. In Figs. 2 and 3, the magnetic field in the mid-plane $z = 0.5$ is shown for $Re_m = 0.1$, $100, 400, 1000$ and the gradual evolution from diffusive transport to convective transport is displayed.

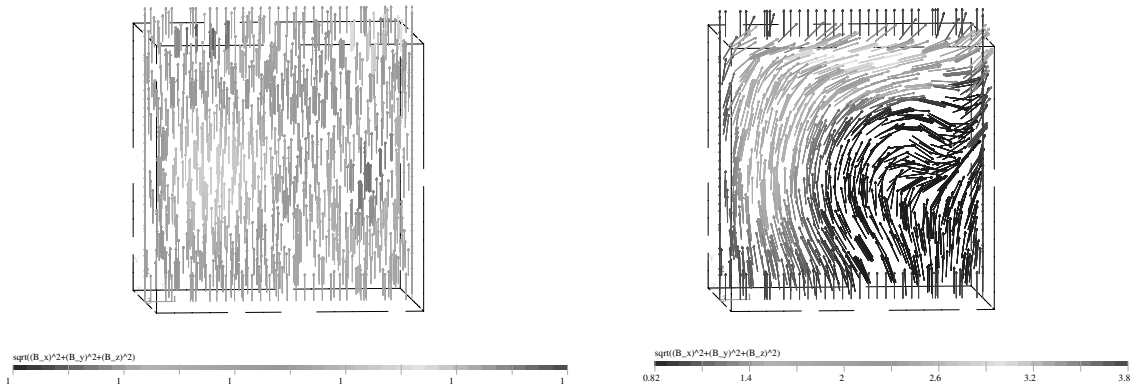

Fig. 2. Magnetic field at the mid-plane $z = 0.5$; From left to right $Re_m = 0.1$, 100.

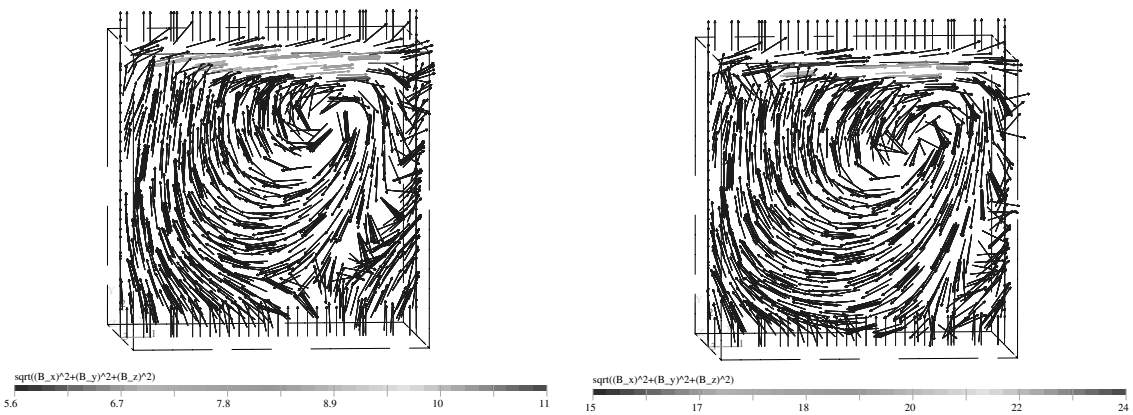

Fig. 3. Magnetic field at the mid-plane $z = 0.5$; From left to right $Re_m = 400$, 1000.

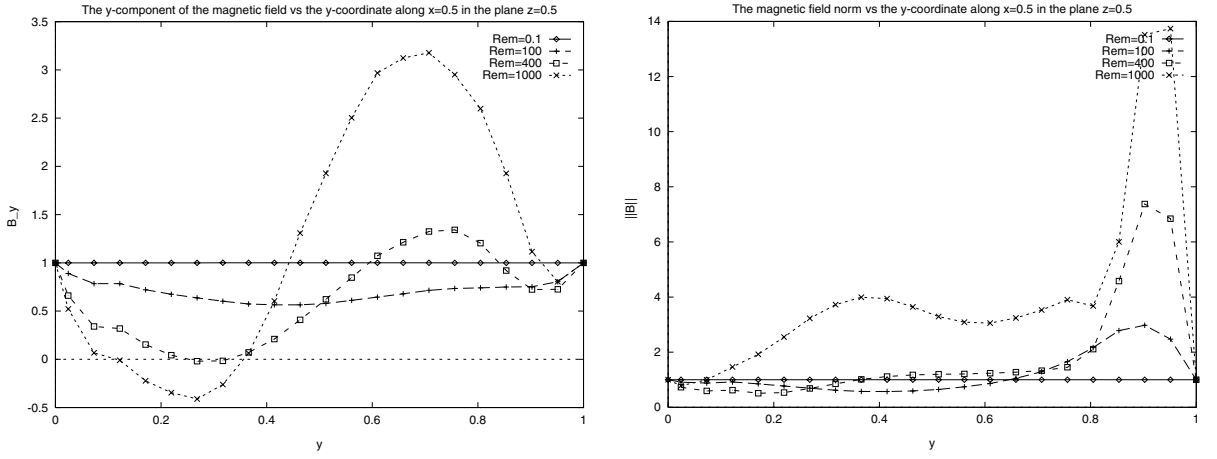

Fig. 4. The magnetic field along the median $x = 0.5$; left: the y-component of the magnetic field, right: the magnetic vector norm.

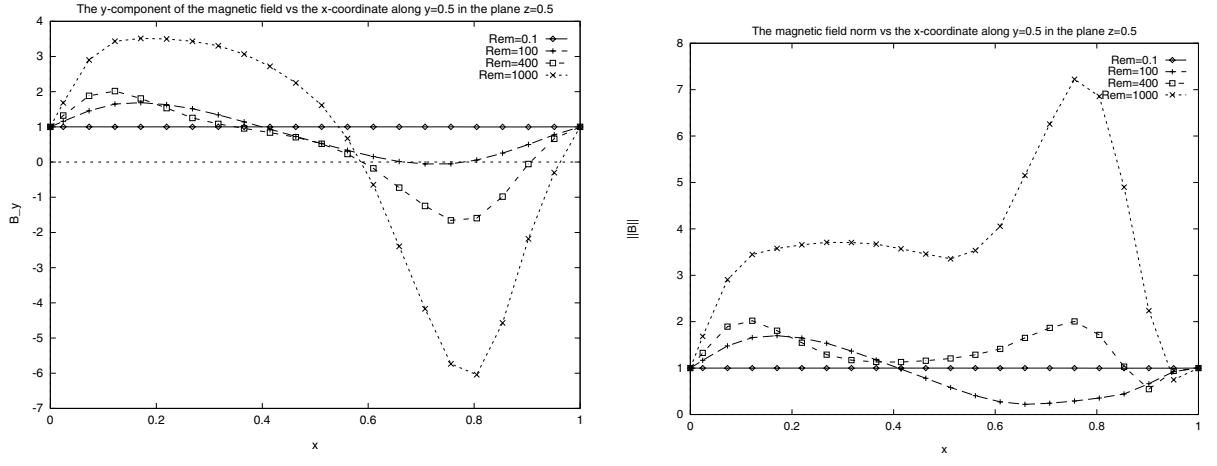

Fig. 5. The magnetic field along the median $y = 0.5$; left: the y-component of the magnetic field, right: the magnetic vector norm.

In Figs. 4 and 5, the magnetic field norm and the y-component of the magnetic field are shown, respectively, along the medians $y = 0.5$ and $x = 0.5$. The convective transport is again shown as the Re_m grows from 0.1 to 1000. Fig. 6 shows the velocity field (given as an input data for this test) norm and the y-component of the velocity along the median $y = 0.5$. Comparing the qualitative behaviors of the velocity (Fig. 6) and of the magnetic field (Fig. 5) gives the ultimate explanation for the statement *the magnetic field freezing in the velocity field.*

5.2. Results for the vector potential formulations

For the vector potential formulations, we first study the stability and convergence of the finite element formulation (44) and (45). Once this first step is carried out, two other numerical tests are presented: a 1D test, where an external magnetic field is applied on a unidirectional fluid flow and a 2D test, where the rotation of a solid cylinder convects the constant imposed magnetic field. These two tests concern the finite element formulation (46).

5.2.1. Stability of the formulation

In order to assess the stability and quality of the finite element formulation (44) and (45), we study this problem in a cubic domain ($0 \leqslant x \leqslant 1$, $0 \leqslant y \leqslant 1$, $0 \leqslant z \leqslant 1$). The velocity vector is fixed to $\mathbf{u} = (1, 1, 1)^{\mathrm{T}}$. The

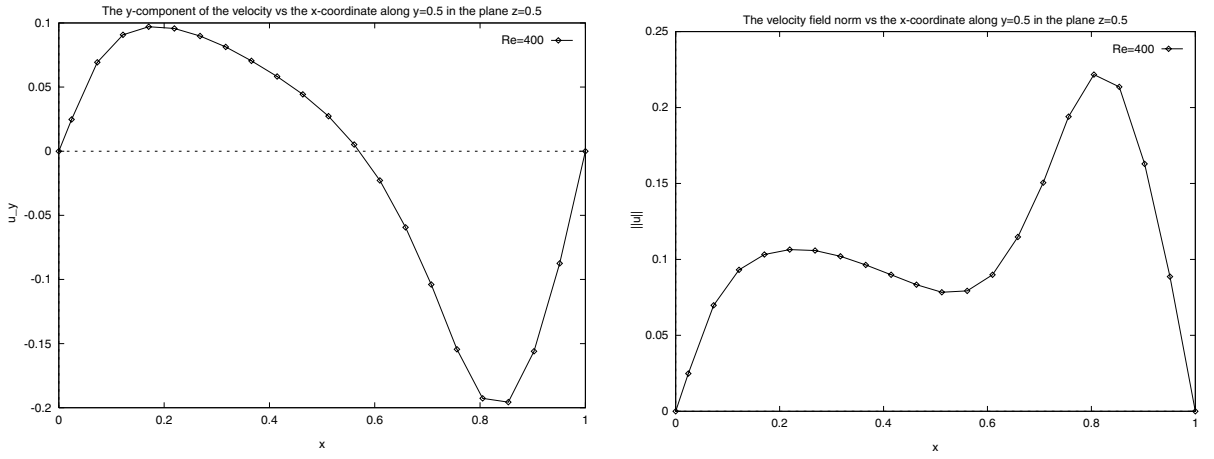

Fig. 6. The velocity field along the median $y = 0.5$; left: the y-component of the velocity field, right: the velocity vector norm.

Dirichlet boundary conditions and the right-hand side vector $\mathbf{f} = (2z - 2\eta + 1, 2z - 2\eta + 1, 1 - 4z, 4)^{\mathrm{T}}$ are imposed in such a way as to reproduce approximately an arbitrary solution of the continuous problem, namely $\mathbf{A} = (x^2, y^2, -2(x + y)z)^{\mathrm{T}}$ and $\phi = x + y + z$. Computations have been performed with $\eta = 0.1$. We compute the mesh variation of the $L_2(\Omega)$-norms of the magnetic vector potential divergence $||\nabla \cdot \mathbf{A}_h||$, the vector potential error $||\mathbf{A}_h - \mathbf{A}||$, the electric scalar potential $||\phi_h||$ and its gradient $||\nabla \phi_h||$. Fig. 7 shows the variation of these norms. The method is stable. The convergence rates (slopes) have been computed for the vector potential. The slopes are around unity for the divergence of the vector potential and around 2 for the vector potential itself.

5.2.2. Uniform flow under a magnetic field

Suppose an electrically conducting fluid domain Ω has a uniform y-component velocity V. An external alternative magnetic field $\mathbf{B}$ with frequency ω, is applied on the fluid domain. Suppose further that $\mathbf{B}$ has only one component along the x direction with B_x being only a function of y: $\mathbf{B} = (B_x(y), 0, 0)$. Then, if one uses the reduced vector potential $\mathbf{A}^*$ formulation, the magnetic field condition $\mathbf{B} = (B_x(y), 0, 0)$ becomes in terms of the reduced potential, $\mathbf{A}^* = \left(0, 0, A_z^*(y)\right)$. The described problem has an analytical solution (Trophime [27]) in terms of the reduced vector potential $\mathbf{A}^*$ which can be written, when the frequency ω is null, as (for simplicity of notation A^* stands for A_z^*)

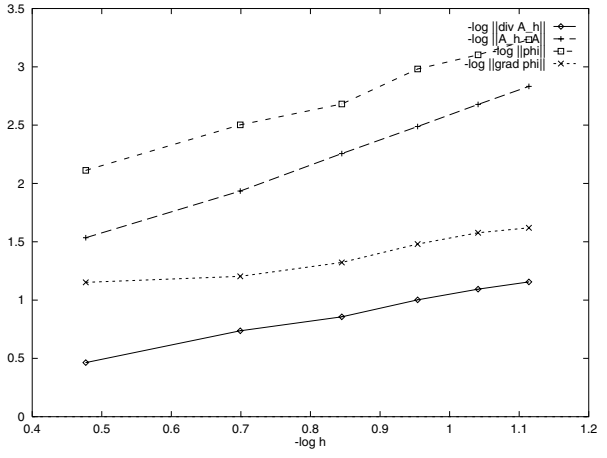

Fig. 7. Different L_2 norms vs the mesh size.

$$A^*(y) = \frac{A_0(e^{Re_m} - 1) + (A_1 - A_0)\left(e^{Re_m y/L} - 1\right)}{e^{Re_m} - 1} \tag{55}$$

with the boundary conditions being:

$$A^*(0) = A_0, \tag{56}$$

$$A^*(L) = A_1. \tag{57}$$

Numerical solutions have been computed for different magnetic Reynolds numbers ($Re_m = 1, 5, 10, 20, 40, 50$). The results show a quite good agreement between computed and analytical solutions (Fig. 8).

5.2.3. Convection of a magnetic field by a rotating velocity field

A very long cylinder of radius r_0 with a conductivity σ is rotating in the xy plane with an angular velocity ω_0. Suppose then that the cylinder is immersed in a uniform magnetic field **B** directed along the x-axis (Fig. 9). The magnetic field lines are then convected by the velocity of the cylinder. The effect of convection is proportional to the magnetic Reynolds number ($Re_m = \mu\sigma\omega_0 r_0^2$). In the limit of infinite Re_m, the magnetic field is expelled out of the cylinder. Assuming the cylinder to be infinite along the z-axis and steady-state

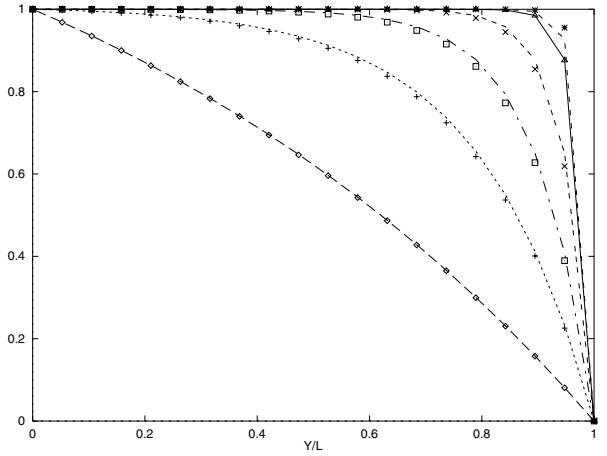

Fig. 8. The reduced potential along the y-axis. Comparison between analytical and numerical solutions for $Re_m = 1, 5, 10, 20, 40, 50$ (from bottom to above).

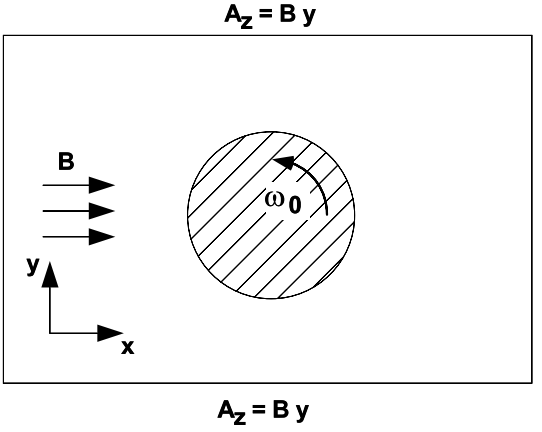

Fig. 9. Geometry for the magnetic field convection by a rotating cylinder.

conditions ($\partial/\partial t = 0$), the vector potential has only one non-trivial component A_z which is a function of x and y. The vector potential problem consists of finding A_z, such that:

$$\nabla^2 A_z - (\mathbf{u} \times \nabla \times \mathbf{A})_z = 0, \quad r > r_0, \tag{58}$$

$$\nabla^2 A_z = 0, \quad r \leqslant r_0. \tag{59}$$

The problem has an analytical solution which has been developed by Moffat [39] and is written as

$$A_z = \mathrm{Im}[Bf(r)\mathrm{e}^{\mathrm{i}\theta}], \tag{60}$$

where

$$f(r) = r + \frac{C}{r}, \quad r > r_0, \tag{61}$$

$$f(r) = DJ_1(pr), \quad r \leqslant r_0 \tag{62}$$

with

$$p = \frac{(1-i)k_0}{\sqrt{2}}, \tag{63}$$

$$k_0^2 = \frac{Re_\mathrm{m}}{r_0^2}. \tag{64}$$

The constants C and D are:

$$C = \frac{r_0[2J_1(pr_0) - pr_0 J_0(pr_0)]}{pJ_0(pr_0)}, \tag{65}$$

$$D = \frac{2}{pJ_0(pr_0)}, \tag{66}$$

The boundary conditions are imposed as in Fig. 9. Numerical solutions have been computed for different magnetic Reynolds number ($Re_\mathrm{m} = 0, 6, 12, 24, 48$). The unstructured nearly uniform mesh consists of 4446 elements and 1600 nodes. Figs. 10 and 11 show the effect of increasing the angular velocity ω_0 on the convection of the magnetic field. These results are in good agreement with the analytical solution. On the other hand, the beginning of the expulsion of the magnetic field is shown in Fig. 12. One can see that as

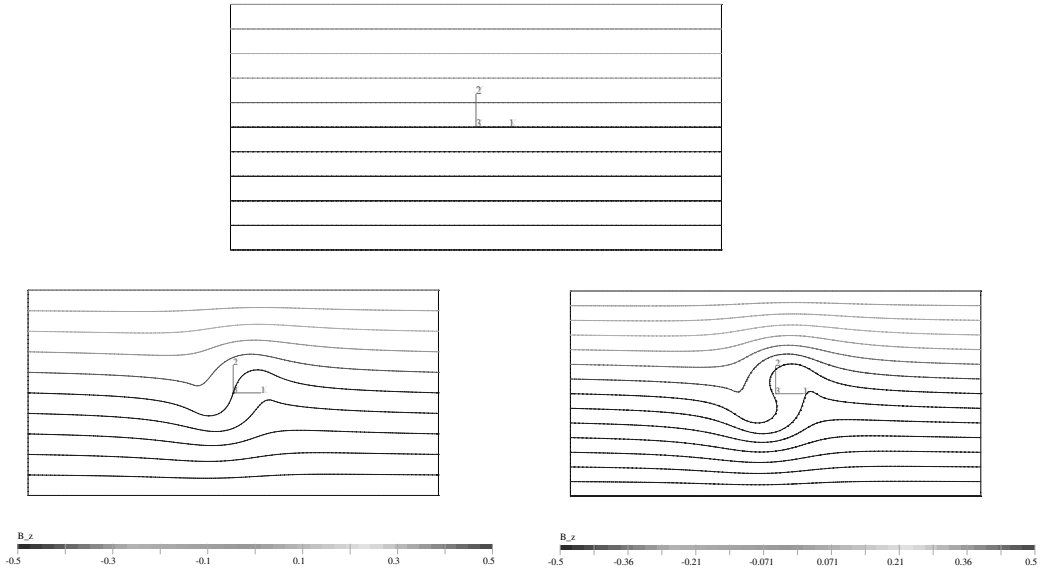

Fig. 10. The isolines of the vector potential $A_z(x, y)$, numerical solutions for $Re_\mathrm{m} = 0$, 6, 12 (from above to bottom right).

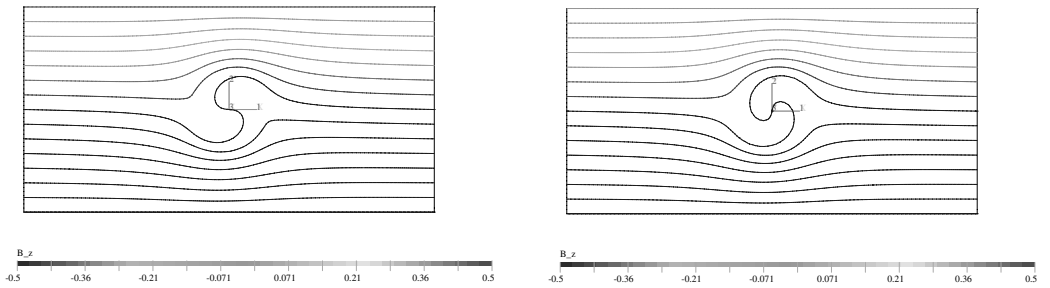

Fig. 11. The isolines of the vector potential $A_z(x, y)$, numerical solutions for $Re_m = 24$, 48 (from left to right).

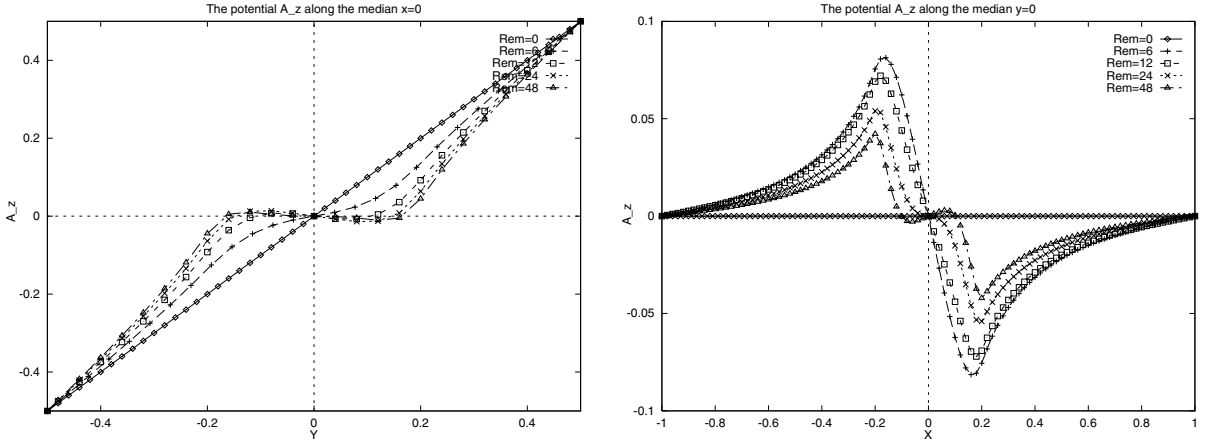

Fig. 12. The vector potential $A_z(x, y)$ for different Re_m numbers, left: along the median $x = 0$, right: along the median $y = 0$.

the magnetic Reynolds number Re_m increases, the vector potential goes to lower values in the vicinity of the cylinder. In these computations, the radius of the cylinder is set to $r_0 = 0.2$ m.

5.3. Results for the $(\mathbf{u}, p, \mathbf{B}, q)$ coupled formulation

For the coupled problem, results are obtained for the lid-driven cavity problem under a constant transversal magnetic field B_0. When the external imposed magnetic field is zero, the problem becomes the classical hydrodynamic lid-driven cavity problem. The cavity is a cubic domain with $(0 \leqslant x \leqslant 1,\ 0 \leqslant y \leqslant 1,\ 0 \leqslant z \leqslant 1)$. The fluid movement in the cavity is induced by the imposed boundary condition $u = u_0$ of the plane $y = 1$ (Fig. 1). The velocity field induces a perturbation of the magnetic field in the fluid domain. Moreover, the interaction between the velocity and the magnetic fields creates the electromagnetic Lorentz forces. These new body forces are responsible for the change of the structure of the flow. The hydrodynamic Reynolds number Re is set to $Re = 10^3$ and a parametric study of the magnetic Reynolds number Re_m and the Hartmann number Ha has been conducted. The unstructured nearly uniform mesh consists of 41 873 elements and 8147 nodes. The parameters of the solution algorithm are set to the following:

- Time step $\Delta t = 5.0$.
- Number of time steps $N = 100$.
- For the ILUT algorithm $lfil = 15$ and $tol = 10^{-09}$.
- For the GMRES algorithm, the number of Krylov basis vectors $m = 8$.
- For the Newton iterations, $niter = 5$.

The Dirichlet boundary conditions are imposed for both the velocity field and the magnetic field, thus expressing the non-slip property at solid walls and the non-perturbation of the external magnetic field by the induced one.

5.3.1. Low magnetic Reynolds numbers

First, we investigate the influence of the Hartmann number Ha at a low magnetic Reynolds number where the magnetic diffusion dominates the magnetic convection. To do so, we set the magnetic Reynolds number to $Re_m = 1$. The Hartmann number is set successively to $Ha = 1, 2, 5, 7, 10, 20, 30$. In the segregated algorithm, the magnetic matrix is computed and decomposed during the first time step and kept constant during all the other time steps. The magnetic problem is solved once at each time step.

In Fig. 13, the convergence history of the residual norm in terms of time steps of the segregated algorithm is shown for different Hartmann numbers.

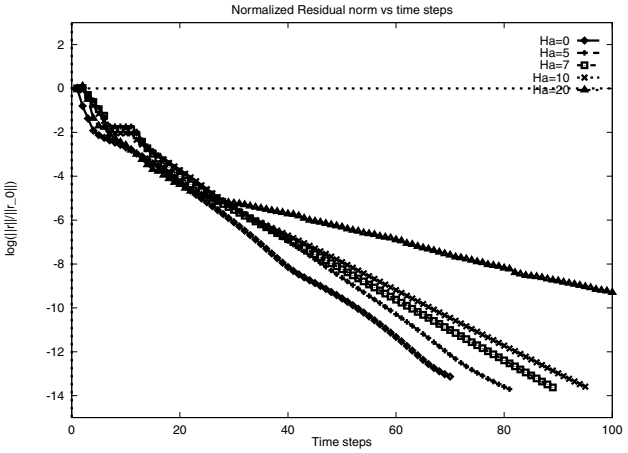

Fig. 13. The convergence history of the segregated algorithm.

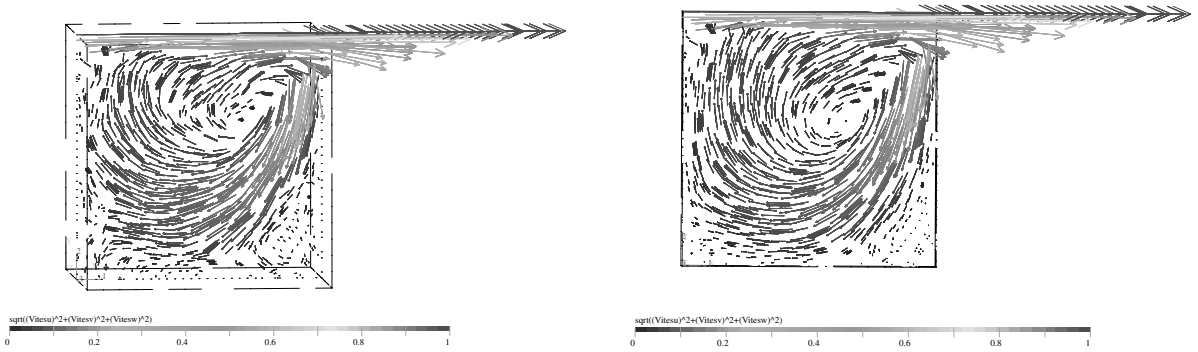

Fig. 14. The velocity field at the mid-plane $z = 0.5$ with $Re = 10^3$ and $Re_m = 1$, left: $Ha = 0$, right: $Ha = 2$.

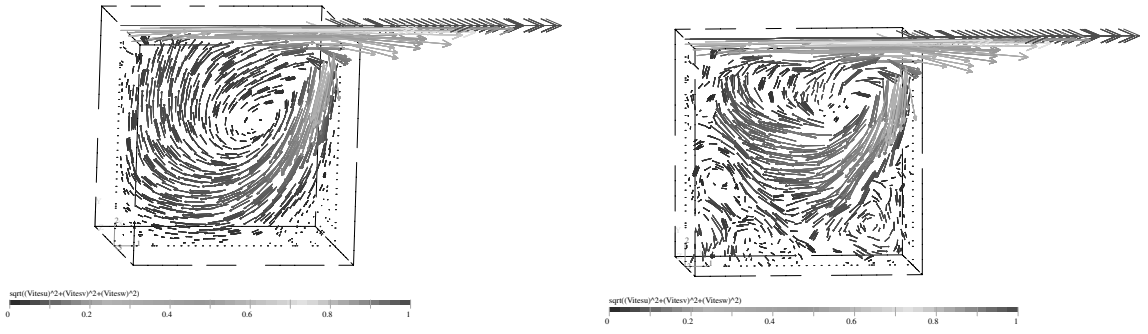

Fig. 15. The velocity field at the mid-plane $z = 0.5$ with $Re = 10^3$ and $Re_m = 1$, left: $Ha = 5$, right: $Ha = 7$.

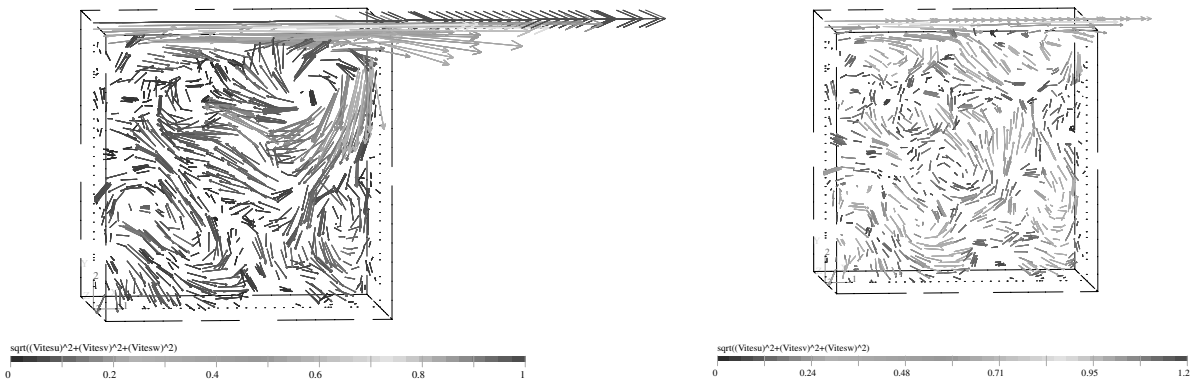

Fig. 16. The velocity field at the mid-plane $z = 0.5$ with $Re = 10^3$ and $Re_m = 1$, left: $Ha = 10$, right: $Ha = 20$.

Figs. 14–16 show the evolution of the velocity field at the mid-plane $z = 0.5$ from $Ha = 0$ to $Ha = 20$. One can observe the dramatic change of the structure of the vortices. When no external magnetic field is applied ($Ha = 0$), there are two vortices: a large central one in the core region (clockwise rotation) and a smaller one in the right bottom corner (counter clockwise rotation). As the Hartmann number Ha becomes greater, the large central vortex becomes more horizontal and eventually breaks into many vortices. The small vortex in the right bottom corner becomes larger. These changes in the vortices structure are due to the increasing effect of the electromagnetic forces which weaken the vortices strength, leading to the breaking of vortices. An analogy exists with the Rayleigh–Benard cell problem under a magnetic field. Seungsoo and Dulikravich [22] showed numerical results confirming the multiplication of initial buoyancy vortices under the effect of a transversal magnetic field.

5.3.2. High Hartmann numbers

When the Hartmann number becomes greater ($Ha > 20$), marching the problem in time does not yield a steady-state solution. The convergence of the algorithm (in terms of time steps) reaches a stagnant plateau; however, the algorithm converges pretty well within a time step (the residual is reduced by 6–7 orders of magnitude). In Fig. 17, a typical behavior of the residual evolution is shown. This can be a sign of the absence of a steady solution under such conditions and the fluid keeps on exhibiting an unsteady behavior as time is increased. In order to show this, we study the behavior of the fluid properties (essentially the different components of the velocity) in terms of time steps, under the following conditions:

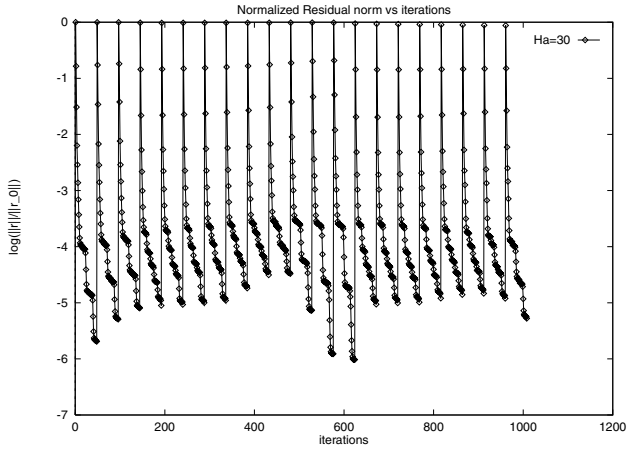

Fig. 17. Typical convergence history for $Re = 10^3$, $Re_m = 1$ and $Ha = 30$.

- Time step $\Delta t = 0.1$.
- Number of time steps $N = 1900$.
- The Hartmann number $Ha = 30$.

Fig. 18 shows the time evolution of the velocity norm for five nodes located in different locations of the domain (Fig. 19). One can see that no steady state is obtained and that the solution continues to oscillate in time. This behavior can be the signature of instabilities developing in the fluid domain due to the effect of the electromagnetic forces which, in this case, are of the same order of magnitude as the convective forces. The absence of predominant forces prevents the development of a pattern of flow leading to a steady-state solution. The study of the stability of the flow is beyond the scope of this thesis; however, a parametric study with the *Ha* number is thought to be necessary for the study of these instabilities that develop within the fluid and for the study of the eventual bifurcations that could be generated.

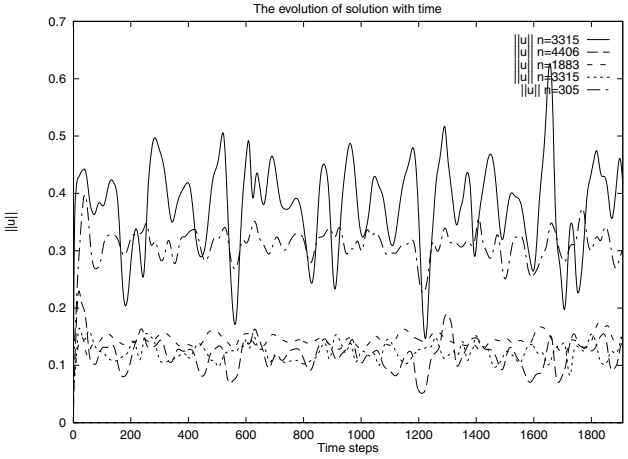

Fig. 18. Transient solution at five different nodes, $Re = 10^3$, $Re_m = 1$ and $Ha = 30$.

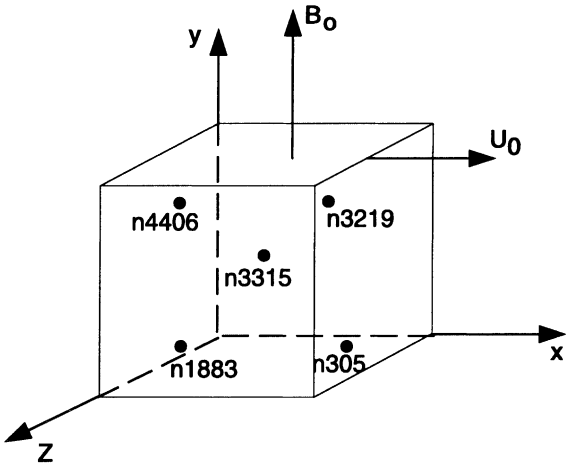

	x coordinate	y coordinate	z coordinate
Node 305	0.88	0.10	0.46
Node 1883	0.15	0.10	0.48
Node 3219	0.85	0.89	0.53
Node 3315	0.50	0.50	0.50
Node 4406	0.18	0.72	0.49

Fig. 19. The nodes considered for the stability: above: location of the nodes on the domain, bottom: coordinates and numbers of the nodes.

5.3.3. Moderate and high magnetic Reynolds numbers

When $Re_m > 1$, the convection of the magnetic field by the velocity one is no longer negligible compared to its diffusion. In such cases, the updating of the magnetic matrix should take place more than once during the time marching process. If the matrix is updated only once, then the algorithm diverges. However, the frequency of the updating depends on the intensity of the Reynolds magnetic number Re_m. In fact, when $Re_m = 10$, it is still possible to converge the algorithm to the machine zero with the magnetic matrix computed and decomposed only at the beginning of the iterative process. When $Re_m = 100$, the matrix is updated every 10 time steps. When $Re_m = 200$, the updating takes place every five time steps. For each of the magnetic Reynolds numbers, the computed velocity and the magnetic fields are given in the plane

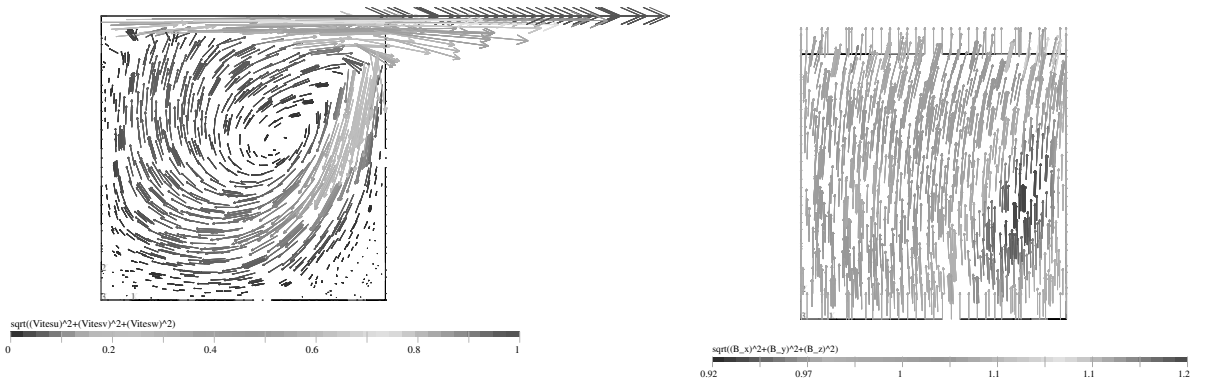

Fig. 20. Results at the mid-plane $z = 0.5$ with $Re = 10^3$, $Re_m = 10$ and $Ha = 10$: left: the velocity field, right: the magnetic field.

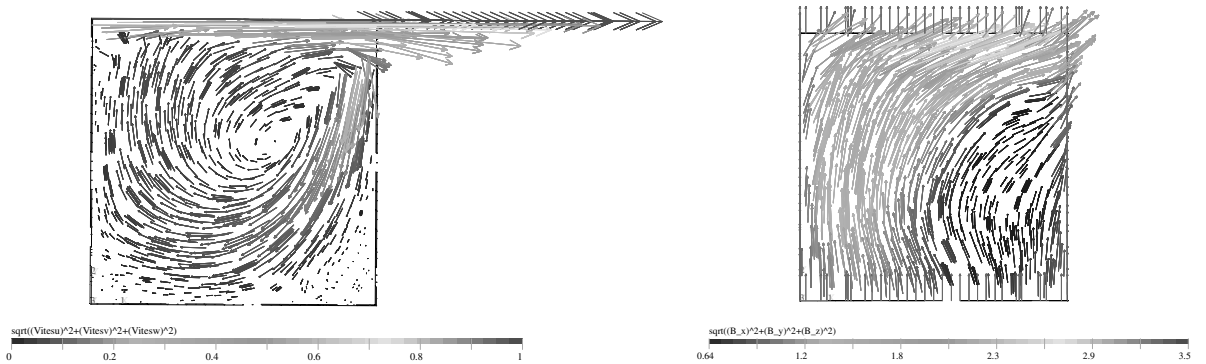

Fig. 21. Results at the mid-plane $z = 0.5$ with $Re = 10^3$, $Re_m = 100$ and $Ha = 10$: left: the velocity field, right: the magnetic field.

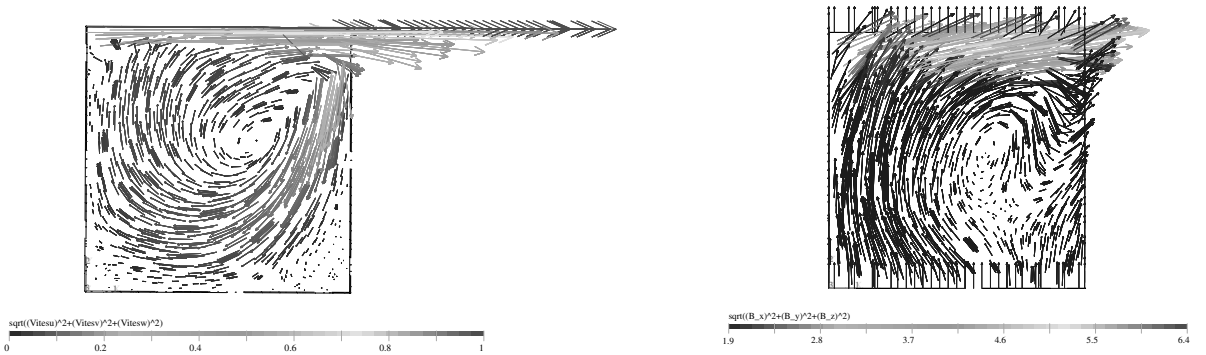

Fig. 22. Results at the mid-plane $z = 0.5$ with $Re = 10^3$, $Re_m = 200$ and $Ha = 10$: left: the velocity field, right: the magnetic field.

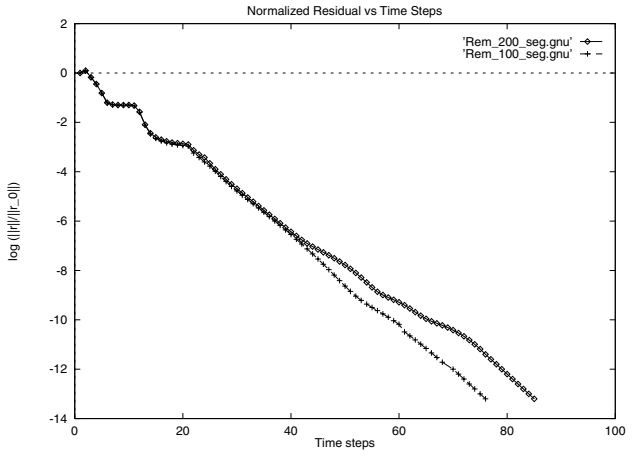

Fig. 23. Convergence history of the segregated algorithm for $Re_m = 100$, 200.

$z = 0.5$ (Figs. 20–22). Fig. 23 shows the convergence history ($Re_m = 100, 200$) of the residual in terms of time steps of the segregated algorithm.

6. Conclusions and future work

A finite element method has been developed in this paper for the solution of 3D MHD equations. The first issue was the selection of an appropriate formulation to correctly solve the magnetic aspects of MHD flows. The selected $(\mathbf{B}, q)$ formulation is conservative in the sense that the local conservation of the magnetic field is accounted for. Furthermore, the finite element approximations used for $\mathbf{B}$ and q are of equal-order type. The stabilized finite element formulations used for the Navier–Stokes and magnetic equations proved able to solve boundary layers and convection dominate flows.

The second issue is the development and assessment of an appropriate algorithm for the solution of the coupled problem. The solution strategy is based on a segregated algorithm which is valid for both high and low Re_m numbers. Numerical experiments proved that this algorithm performs very well, even in the context of high magnetic Reynolds Re_m numbers. The non-linear GMRES algorithm associated with ILUT preconditioning proves to be a very robust and efficient algorithm. When the magnetic Reynolds number is low, the magnetic matrix can be computed only once for all time steps. All subsequent updates of the magnetic variables can be done using the initial decomposition of the magnetic matrix without affecting the convergence rates. However, when the magnetic Reynolds number is high, the matrix has to be updated and decomposed more frequently to guarantee convergence. This frequency depends mainly on the value of Re_m.

Finally, we would like to comment on the somewhat inadequate way the magnetic boundary conditions were handled for the high Re_m cases. In fact, when Re_m is high, there is no reason to suppose that the external magnetic field is not affected by the induced magnetic field. The appropriate way to solve such a problem is to solve the MHD equations in two domains. The first domain is the conducting fluid, where the MHD equations are written as shown in Section 1. The second domain, surrounding the conducting domain, is non-conducting by definition and is large enough to suppose that the induced magnetic field at its boundaries is null. The MHD equations in this domain are written without the convective term, since the velocity is nil. At the boundaries between the two domains, and since in MHD the permeability is constant, the magnetic field is continuous over the interface and no boundary conditions have to be specified.

References

[1] P.L. Roe, D.S. Balsara, Notes on the eigensystem of magnetohydrodynamics, SIAM J. Appl. Math. 56 (1) (1996) 57.
[2] K.G. Powell, Solution of Euler and magnetohydrodynamic equations on solution-adaptative Cartesian grids, Von Karman Institute for Fluid Dynamics, Lecture Series 1996-06, Computational Fluid Dynamics, Concordia University, Montreal, 1996.

[3] J.S. Walker, in: H. Branover, P.S. Likoudis, M. Moon (Eds.), Laminar Duct Flows in Strong Magnetic Fields: Liquid–Metal Flows and Magnetohydrodynamics, vol. 2, American Institute of Aeronautics and Astrodynamics, New York, 1986, p. 3.
[4] T.Q. Hua, J.S. Walker, MHD flow in rectangular ducts with inclined non-uniform transverse magnetic field, Fusion Engrg. Design 27 (1995) 703.
[5] S. Cuevas, B.F. Picologlou, J.S. Walker, G. Talmage, Liquid–metal MHD flow in rectangular ducts with thin conducting or insulating walls: laminar and turbulent solutions, Int. J. Engrg. Sci. 35 (5) (1997) 485.
[6] J.I. Ramos, N.S. Winowich, Finite difference and finite element methods for MHD channel flows, IJNMF 11 (1990) 907.
[7] R. Scandiuzzi, B.A. Schrefler, F.E.M. in steady MHD duct flow problems, IJNME 30 (1990) 647.
[8] O. Biro, K. Preiss, On the use of magnetic vector potential in the finite element analysis of three-dimensional eddy currents, IEEE Trans. Magnetics 25 (4) (1989) 3145.
[9] Y.R. Fautrelle, Analytical and numerical aspects of electromagnetic stirring induced by alternating magnetic fields, JFM 102 (1981) 405.
[10] A.J. Mestel, Magnetic levitation of liquid metals, JFM 117 (1982) 27.
[11] S.D. Lympany, J.W. Evans, R. Moreau, Magnetohydrodynamic effects in aluminium reduction cells, in: H.K. Moffat, M.R.E. Proctor (Eds.), Metallurgical Applications of Magnetohydrodynamics, Proceedings of a Symposium of the International Union of the Theoretical and Applied Mechanics, Cambridge, UK, 6–10 September 1982, The Metals Society, London, 1984, p. 15.
[12] O. Besson, J. Bourgeois, P.A. Chevalier, J. Rappaz, R. Touzani, Numerical modeling of electromagnetic casting processes, JCP 92 (1991) 482.
[13] H.J. Conraths, Eddy current and temperature simulation in thin moving metal strips, IJNME 39 (1996) 141.
[14] P. Masse, Y. Fautrelle, A. Gagnoud, Coupled methods for 3D coupled problems, 10 years of experiments in MHD, IEEE Trans. Magnetics 28 (1992) 1275.
[15] C. Emson, J. Simkin, An optimal method for 3D eddy currents, IEEE Trans. Magnetics 19 (1983) 2450.
[16] B. Jiang, J. Wu, L.A. Povinelli, The origin of spurious solutions in computational electromagnetics, NASA-TM-106921, E-9633, ICOMP-95-8, 1995.
[17] H. Brezis, Analyse Fonctionnelle, Masson, Paris, 1983.
[18] L.D. Landau, E.M. Lifshitz, L.P. Pitaevskii, Electrodynamics of Continuous Media, Pergamon Press, Oxford, 1984.
[19] N. Ben Salah, A. Soulaimani, W.G. Habashi, M. Fortin, A conservative stabilized finite element method for the magnetohydrodynamic equations, IJNMF 29 (1999) 535.
[20] N. Ben Salah, A. Soulaimani, W.G. Habashi, M. Fortin, A conservative stabilized finite element method for the magnetohydrodynamic equations, in: S.N. Alturi, G. Yagawa (Eds.), Advances in Computational Engineering Science, International Computational Engineering and Science 97, Tech Science Press, Forsyth, Georgia, 1997, p. 269.
[21] A. Sterl, Numerical simulation of liquid–metal MHD flows in rectangular ducts, JFM 216 (1990) 161.
[22] L. Seungsoo, G.S. Dulikravich, Magnetohydrodynamic steady flow computations in three dimensions, IJNMF 13 (1991) 917.
[23] G.S. Dulikravich, V. Ahuja, L. Seungsoo, Three-dimensional control of crystal growth using magnetic fields, in: Proceedings of SPIE, The International Society for Optical Engineering Proceedings of Smart Structures and Materials, vol. 1916, 1993.
[24] S.S. Sazhin, M. Makhlouf, Solution of magnetohydrodynamic problems based on a conventional computational fluid dynamics code, IJNMF 21 (1995) 433.
[25] J.S. Peterson, On the finite element approximation of incompressible flows of an electrically conducting fluid, Numer. Methods Partial Diff. Equations 4 (1988) 57.
[26] L.T.R. Gardner, G.A. Gardner, A two-dimensional bi-cubic and B-Spline finite element: used in a study of MHD duct flow, Comput. Methods Appl. Mech. Engrg. 124 (1995) 365.
[27] C. Trophime, Modélisation Numérique du Couplage agnétohydrodynamique (MHD) Fort, Application à la Propulsion MHD Navale, Thèse de Doctorat à l'Institut National Polytechnique de Grenoble, France, 1995.
[28] N. Ben Salah, A finite element method for the fully coupled magnetohydrodynamics, Ph.D. Thesis at Concordia University, Montreal, Canada, 1999.
[29] T. Tanahashi, Y. Oki, Numerical analysis of natural convection of thermo-electrically conducting fluids in a square cavity under a uniform magnetic field, JSME International Journal 39 (1996) 508.
[30] F. Brezzi, J. Pitkaranta, On the stabilization of finite element approximations of the stokes problem, in: W. Hackbusch (Ed.), Efficient Solutions of Elliptic Systems, vol, 10, Notes on Numerical Fluid Mechanics, Viewig, Wiesbaden, 1984, p. 11.
[31] F. Brezzi, M. Fortin, Mixed and Hybrid Finite Element Methods, Springer Series in Computational Mathematics, vol. 15, Springer, Berlin, 1991.
[32] T.J.R. Hugues, L. Franca, M. Ballestra, A new finite element formulation for computational fluid dynamics: V circumventing the Babuska–Brezzi condition: a stable Petrov Galerkin formulation of the stokes problem accommodating equal order interpolation, Comput. Methods Appl. Mech. Engrg. 59 (1986) 85.
[33] T.J.R. Hugues, L. Franca, G.M. Hubert, A new finite element formulation for computational fluid dynamics: VIII the Galerkin/least squares method for advective–diffusive equations, Comput. Methods Appl. Mech. Engrg. 73 (1989) 173.
[34] L.C. Dutto, On the iterative methods for solving linear systems of equations, Revue Européenne des Élements Finis 2 (1993) 423.
[35] Y. Saad, M.H. Schultz, GMRES: A generalized minimal residual algorithm for solving non-symmetric linear systems, SIAM J. Sci. Stat. Comput. 7 (1986) 856.
[36] Y. Saad, Iterative Methods for Sparse Linear Systems, PWS Publishing, Boston, 1996.
[37] Y. Saad, ILUT: a dual threshold incomplete ILU factorization, Numer. Linear Algebra Appl. 1 (1994) 387.
[38] Y. Saad, Numer. Linear Algebra Appl. 7 (1986) 856.
[39] H.K. Moffat, Magnetic Field Generation in Electrically Conducting Fluids, Cambridge University Press, London, 1983.